PHASE EQUILIBRIA IN THE $LiF-AlF_3-Na_3AlF_6$ SYSTEM

by

David P. Stinton

Thesis submitted to the Graduate Faculty of the

Virginia Polytechnic Institute and State University

in partial fulfillment of the requirements for the degree of

MASTER OF SCIENCE

in

Ceramic Engineering

APPROVED:

Dr. J. J. Brown, Jr., Chairman

Dr. W. C. Hackler

Dr. L. H. Slack

ACKNOWLEDGEMENTS

The author wishes to express his sincere appreciation to his wife, , for her encouragement and moral support during the course of this work.

The author also wishes to thank the chairman of his graduate committee, , for his guidance, constructive criticism and friendship during the past year.

and also contributed greatly to the writers development in the last year of work and study.

This work was supported by an Alcoa Foundation grant.

TABLE OF CONTENTS

LIST OF TABLES

LIST OF FIGURES

I. INTRODUCTION

Aluminum is a very important industrial material that weighs only one-third as much as iron, brass, or copper and, consequently has many important structural applications. Unlike other typical metals, aluminum has a very high affinity for oxygen; so high, in fact, that it can not be produced by direct smelting of its ores. (The temperature required to reduce aluminum oxide, Al_2O_3, to the pure metal would be so high that the aluminum produced would immediately vaporize.) Today aluminum is manufactured by a two step process; first Al_2O_3 is extracted from an aluminum mineral, usually bauxite, and then aluminum is produced by electrolysis using an electrolyte which consists of alumina dissolved in a molten fluoride mixture. This process often referred to as the Hall process was developed simultaneously but independently by C. M. Hall and L. T. Heroult in 1886.

The electrolysis of aluminum is often referred to as a three-layer process because it utilizes an anode layer, a cathode layer, and an electrolyte layer. The cathode is a steel pot usually about 25 feet long, 12 feet wide, and 3 feet deep which is lined with carbon insulation 6 to 10 inches thick. A series of large pressed carbon rods dipped into the molten bath act as the anode. The electrolyte is a layer of molten fluoride salts which separate the anode from the cathode.

The production of aluminum starts by pouring molten electrolyte into the steel cathode container. The electrolyte consists mostly of cryolite (Na_3AlF_6) with small amounts of lithium fluoride and aluminum fluoride added to increase the electrical conductivity and decrease the melting temperature of the mixture. Alumina is dissolved in the electrolyte in amounts up to about 5 wt %. A very high current (50,000-125,000 amps) is applied to a group of cells which are connected in series.[1] (Series connections are used because the pots operate between 4 and 7 volts.) The current causes alumina to be decomposed with molten aluminum being deposited on the sides of the cathode and collecting in the bottom of the steel pot. Oxygen is deposited on the cathode causing the carbon to oxidize forming CO_2 plus 10-50% CO. As aluminum is produced the alumina content becomes depleted, therefore alumina must continually be added. The cell will continue to produce aluminum until only about 2% alumina is left. Below 2% the electrolyte no longer wets the anode so current cannot pass from the anode to the electrolyte and the voltage across the cell increases significantly. This series of events is called an anode effect and it is very detrimental because excess CO is produced increasing the consumption of the anode and wasting electrical energy. The anode effect may be stopped by breaking the crust of the electrolyte and adding powdered alumina but this is difficult because the specific gravity of alumina is 4.0 while that of the electrolyte is 2.095 and molten aluminum is 2.29. The alumina added

must be dissolved in the electrolyte before it can settle to the bottom. This is done by vigorously stirring the electrolyte. Bubbles from the anode and a strong magnetic effect help agitate the electrolyte. Alumina will be dissolved more readily if the density of the electrolyte is increased, and, therefore, small amounts of CaF_2 are added. This addition must be kept below 15% or the density of the aluminum metal and the electrolyte will be too close causing aluminum to float to the surface and short out the cell.

During the production of aluminum the anodes are continually consumed. The anodes must be fed into the bath at a rate keeping them 4 to 5 inches above the molten metal. Carbon is consumed at a rate of 0.6 to 0.8 lbs of carbon/lb of aluminum produced.[1] The electrolyte is not decomposed during this process but 3-5 wt % is lost during production. Alumina is decomposed at a rate of about 2 lbs/lb of aluminum.[1] Molten aluminum can be removed from the bottom of the cell by tapping, ladling or siphoning.

The overall reaction that takes place within the molten fluoride electrolyte during the smelting of aluminum is

$$Al_2O_3 + 3/2C = 3/2CO_2 + 2Al$$

The exact solution mechanism and electrode reactions are not known but two theories have been reported.

The first theory[2,3,4,5,6,7,8] proposes that the major ionic species in the electrolyte are Na^+, AlF_6^{3-}, and AlO_2^- with partial dissociation of AlF_6^{3-} to AlF_4^- and F^-, and the possible dimerization

of some AlO_2^- to form $Al_2O_4^{2-}$. The proposed solution mechanism with these ionic species is

$$3F^- + Al_2O_3 = 3/2AlO_2^- + 1/2AlF_6^{3-}$$
$$3F^- + Al_2O_3 = 3/4Al_2O_4^{2-} + 1/2AlF_6^{3-}$$

The reaction at the anode then becomes

$$3/2AlO_2^- + 3/2C + 9F^- = 3/2AlF_6^{3-} + 6e^-$$

with the reaction at the cathode being

$$2AlF_6^{3-} + 6e^- = 2Al + 12F^-$$

The overall electrode reaction equation becomes

$$3/2C + 3/2AlO_2^- + 1/2AlF_6^{3-} = 2Al + 3/2CO_2 + 3F^-$$

The second theory[6,9,10,11] uses the same ionic species as the first except AlO_2^- is replaced by oxyfluoride complexes such as $AlOF_2^-$, $AlO_2F_2^{3-}$, and $Al_2O_2F_4^{2-}$. The solution reactions are

$$5/2AlF_6^{3-} + Al_2O_3 = 3/2AlO_2F_2^{3-} + 3AlF_4^-$$
$$AlF_6^{3-} + Al_2O_3 = 3AlOF_2^-$$
$$AlF_6^{3-} + Al_2O_3 = 3/2Al_2O_2F_4^{2-}$$

The reaction at the anode with these reactions is

$$3AlOF_2^- + 3/2C + 12F^- = 3/2CO_2 + 3AlF_6^{3-} + 6e^-$$

The cathode reaction is

$$2AlF_6^{3-} + 6e^- = 2Al + 12F^-$$

These electrode reactions lead to the same overall reactions as the first theory.

Scientists' support is divided between these two theories because strong evidence can be cited for either reaction mechanism.

The Hall process requires tremendous amounts of energy to operate because the smelting pots operate at a temperature near 950°C. The process as it was used in 1939 required 12 kilowatt hours of electricity to produce one pound of aluminum[12]. Refinements in the process since 1939 have reduced the energy consumption to an average of 8 kilowatt hours per pound of aluminum. With the soaring cost and frequent shortages of electrical energy it is more important than ever to reduce the amount of energy required in producing aluminum. One way of accomplishing this is to use an optimum molten bath composition. The composition now used is often determined by trial and error because of the incompleteness of available data on the solubility of alumina in the bath and the bath's melting temperature. An investigation of the liquidus-solidus equilibria in the $LiF-AlF_3-Na_3AlF_6$ system will yield helpful information in reducing the bath's melting temperature as well as providing preliminary information on the solubility of alumina in the molten fluoride bath.

II. LITERATURE REVIEW

The most important component of the molten fluoride electrolyte is Na_3AlF_6 (the mineral cryolite). This compound exists in two polymorphic forms. The low temperature α phase has a monoclinic crystal structure that is stable up to a temperature between 558 and 570°C. In this temperature range the low temperature α phase undergoes a rapid reversible inversion forming the cubic, high temperature β polymorph[13-15]. The melting point of the cubic polymorph was determined to be between 997 and 1000°C by early workers[16-24]. Using improved methods more recent research has found the melting point to be closer to 1010°C. In a very recent study, using sealed platinum sample containers, careful control of chemical impurities, and the quenching technique, the melting point for pure Na_3AlF_6 was found to be 1012 ± 2°C[25].

The melting point of cryolite is difficult to determine because it tends to dissociate to NaF and $NaAlF_3$ close to its melting point[2-4,26]. Measurements of the apparent heat of fusion of cryolite give a value of 27.8 Kcal/mole[27-28]. It was recently shown that this value contains a contribution from both melting and dissociation. The true measure of the heat of fusion with no dissociation is 19.9 Kcal/mole[2].

The other two end members of the ternary system are lithium fluoride and aluminum fluoride. Lithium fluoride exists in only

one crystalline modification. It has the cubic NaCl type structure and melts at 847°C. Aluminum fluoride also exists in one crystalline form which is rhombohedral and melts at 1291°C.

1) Binary Diagrams

a) The Na_3AlF_6-AlF_3 System

The equilibrium diagram of Na_3AlF_6-AlF_3 has been investigated many times[3,18,23,29-31]. It is generally agreed that one compound $Na_5Al_3F_{14}$ (the mineral chiolite) is stable in the system. At 741°C it decomposes to yield cryolite and a liquid giving rise to a peritectic reaction isotherm[32]. The liquid in equilibrium at the peritectic contains 30% AlF_3 and 70% Na_3AlF_6. The equilibrium solid is pure cryolite with no solid solution of AlF_3. A recent version of this diagram is shown in Figure 1. Numerous researchers have also reported a second compound ($NaAlF_4$) to exist in the system which has recently been shown to exist metastably[3,18,23,31,32]. This was found by observing that $NaAlF_4$ was present in samples quenched from an all liquid region. If a sample was quenched from just below the solidus temperature no $NaAlF_4$ was detected by x-ray examination. This was confirmed by optical examination of quenched samples. These facts suggest that $NaAlF_4$ crystallizes metastably from the melt.

A eutectic reaction exists in the system Na_3AlF_6-AlF_3 at 694°C and 61.5 mole % AlF_3 where chiolite and aluminum fluoride are in

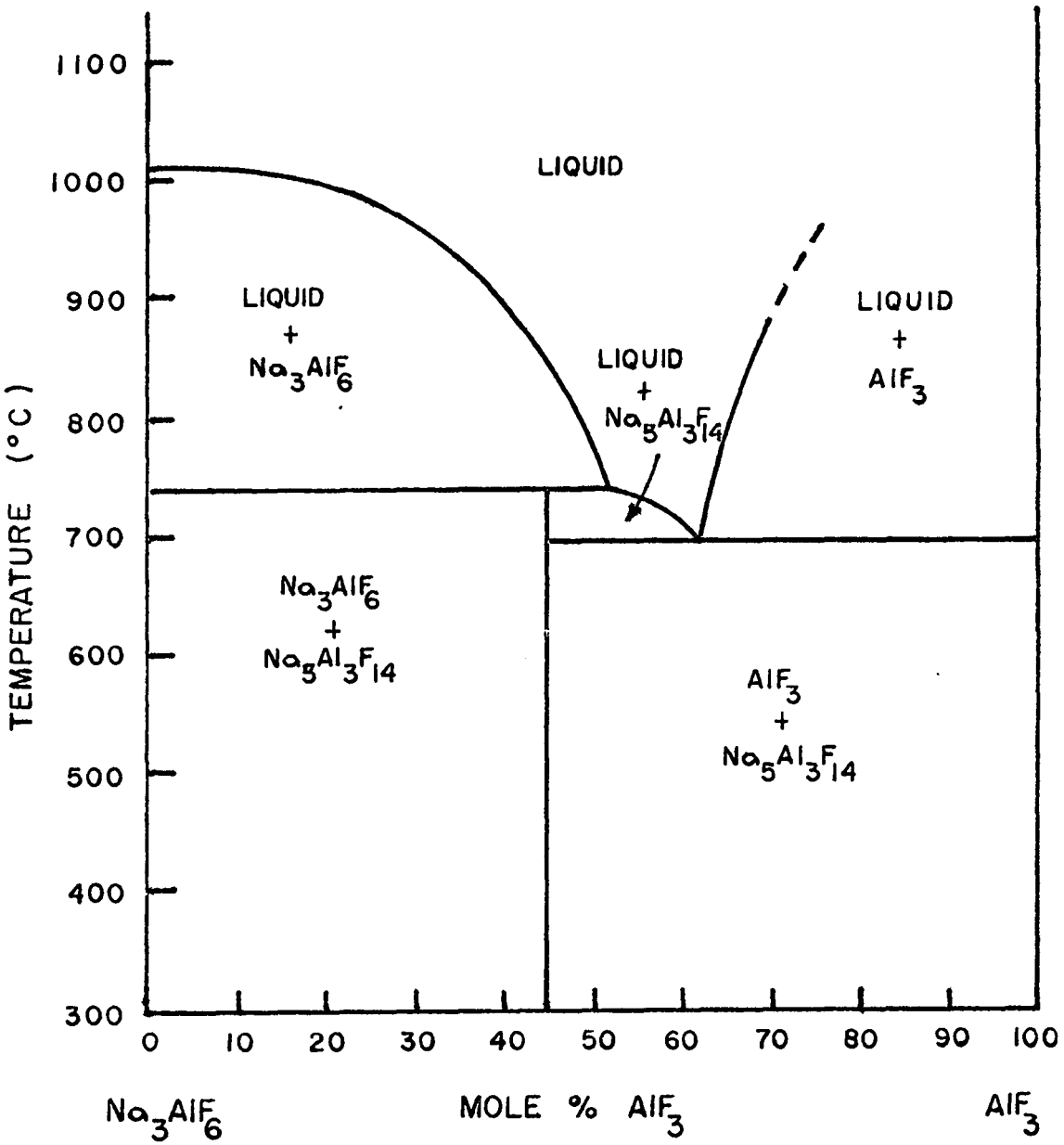

FIGURE 1. THE Na_3AlF_6-AlF_3 PHASE DIAGRAM[32]

equilibrium with liquid. Both of these crystalline phases are pure with no indication of intersolubility thus far reported.

b) The $LiF-AlF_3$ System

One stable compound exists in the binary system $LiF-AlF_3$[33], Li_3AlF_6 (lithium cryolite) which exists in three stable polymorphic forms[34]. The low temperature β phase is orthorhombic and changes to the tetragonal γ phase at 510°C. At 597°C the cubic δ polymorph becomes stable. A fourth ε phase[15] of lithium cryolite becomes stable above 700°C and melts congruently at 790°C.

Between lithium fluoride and lithium cryolite there is a simple eutectic reaction isotherm at 713°C[35]. The eutectic point occurs at 15 mole % AlF_3 and no solid solution of either crystalline phase has been observed. There is also a eutectic reaction isotherm between lithium cryolite and aluminum fluoride at 710°C[35]. The equilibrium liquid at this eutectic contains 36 mole % AlF_3. There has been no solid solution reported for either of these crystalline phases. An accepted diagram of the system is shown in Figure 2.

c) The Na_3AlF_6-LiF System

Equilibrium diagrams of the system Na_3AlF_6-LiF have been reported by numerous researchers[30,36,37]; unfortunately these diagrams do not agree completely. All agree that a eutectic reaction exists somewhere between 84 and 87 mole % LiF at a temperature between 693 and 703°C. Large discrepancies exist in the amount of

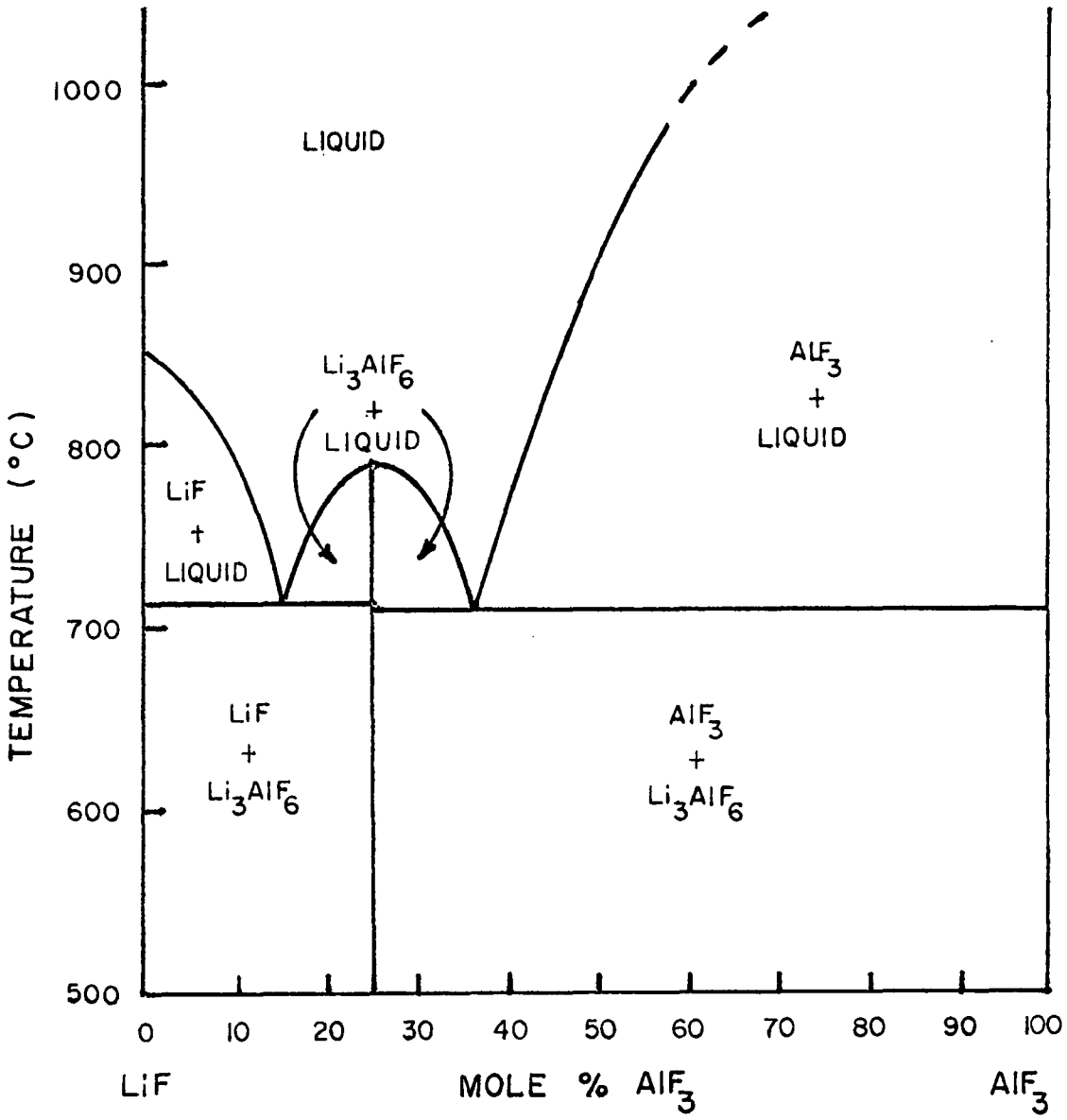

FIGURE 2. THE LIF-AlF_3 PHASE DIAGRAM[35]

intersolubility between the solid phases present at the eutectic temperature. Most studies show simple eutectic systems with no solid solution; however, one investigation reported extensive solid solution to exist from 0 to about 70 mole % LiF[37]. A very small solid solution region has also been reported on the LiF side of the diagram. More recent work done by Foster examined the refractive index of the solid in equilibrium with liquid at various temperatures[38]. He found that the refractive indices changed indicating solid solution regions extending to 13% LiF and 92% LiF at the eutectic reaction isotherm. He found the eutectic at 84% LiF and 695°C. The diagram proposed by Foster is shown in Figure 3.

d) The Na_3AlF_6-Li_3AlF_6 Binary Join

The binary system Na_3AlF_6-Li_3AlF_6 divides the ternary system Na_3AlF_6-AlF_3-LiF in two parts. This binary diagram has been studied many times, but there is little agreement between investigators. In 1937 Drossback studied the system and concluded that it contained a continuous solid solution series with a thermal minimum at 70 mole % Li_3AlF_6 and 710°C[39]. He showed the solidus to fall within 10 to 15° of the liquidus curve. A study in 1957 by Mashovets and Petrov showed a simple eutectic system with no solid solution[40]. They found the eutectic at 710° and 70.5% Li_3AlF_6. Rolin and Muhlethaler studied the system in 1964 and found solid solution extending to the eutectic on the Li_3AlF_6 side of the diagram and to 36 mole % near Na_3AlF_6[41]. Two additional studies have been completed since 1964.

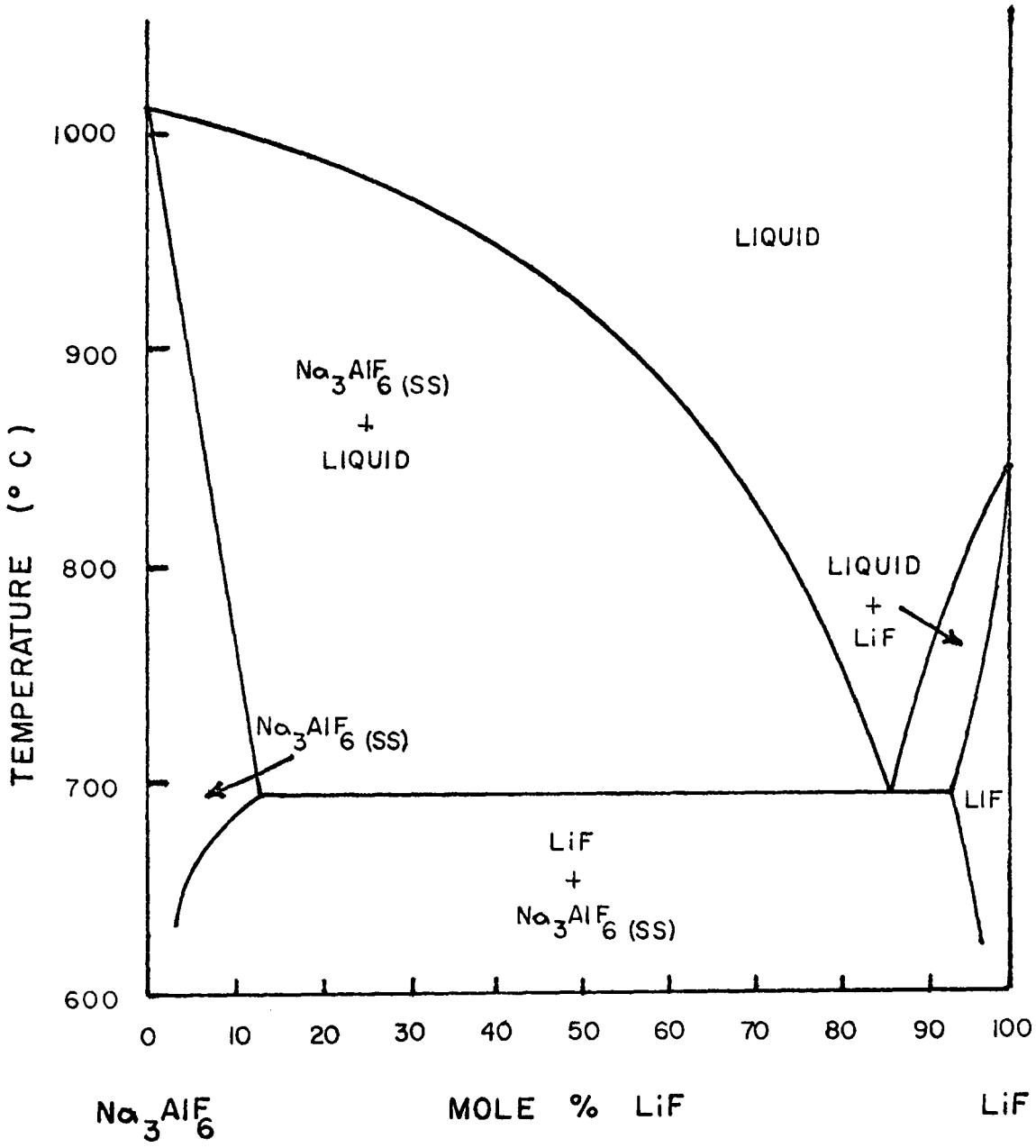

FIGURE 3. THE Na_3AlF_6-LiF PHASE DIAGRAM[38]

The high temperature results of Garton and Wanklyn's[15] work agree with those of Rolin and Muhlethaler. Garton and Wanklyn found the mineral cryolithionite ($Na_3Li_3Al_2F_{12}$) to be a nonstoichiometric solid solution and decompose to Li_3AlF_6 and a phase of Na_3AlF_6 at 680°C. They also found the compound Na_2LiAlF_6 to exist stably up to 500°C. The normal progression of polymorphic changes was also reported. Garton and Wanklyn's version of the diagram is shown in Figure 4. A study in 1970 by Holm and Holm[42] confirmed the high temperature results of Drossbach. They found a complete solid solution series with a thermal minimum at 64 mole % of Li_3AlF_6 and 710°C. The subsolidus equilibria show both cryolithionite and Na_2LiAlF_6 to be stable up to about 500°C. All of these proposed diagrams show liquidus curves that agree very well. They show a thermal minimum or eutectic near 65 mole % Li_3AlF_6 and 710°C. The subsolidus relations are not at all clear at this time.

2) Ternary Diagram

Only one portion of the ternary system Na_3AlF_6-AlF_3-LiF has been studied previously. This is the Li_3AlF_6-Na_3AlF_6-LiF portion which was studied by Holm and Holm in 1973[33]. They discovered a ternary eutectic at 684°C and 83% LiF, 7% AlF_3 and 10% Na_3AlF_6.

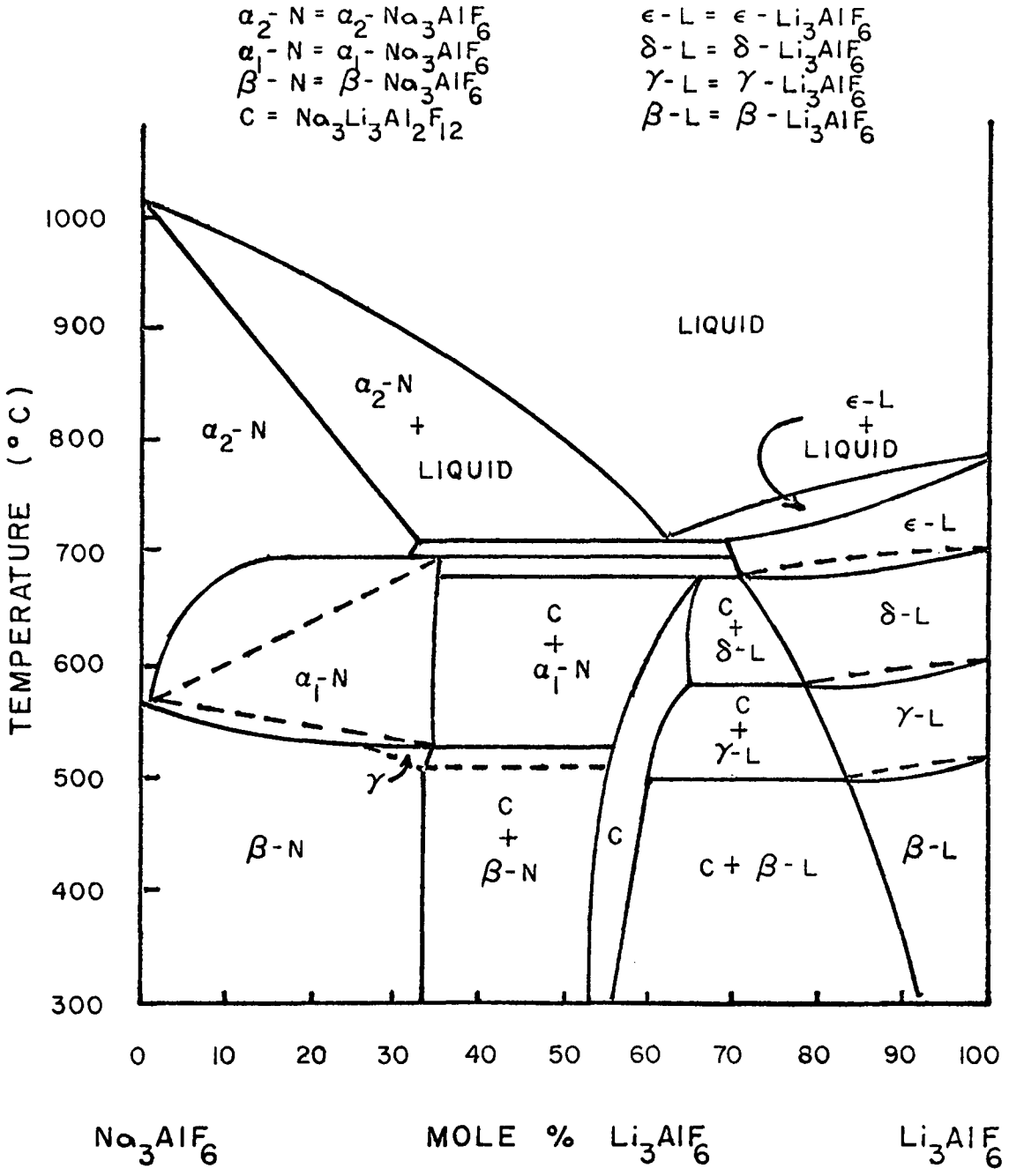

FIGURE 4. THE Na_3AlF_6 - Li_3AlF_6 PHASE DIAGRAM[15]

III. EXPERIMENTAL PROCEDURE

1) Materials

Starting materials used in the study of the Na_3AlF_6-AlF_3-LiF system were reagent grade lithium fluoride*, aluminum fluoride trihydrate**, and hand picked natural Greenland cryolite***. A weight loss factor for aluminum fluoride trihydrate ($AlF_3 \cdot 3H_2O$) was calculated by heating a small amount of sample to various temperatures between 300 and 700°C. These samples were in open fused silica crucibles and left for 24 hours. The weight loss factor closely agreed with the theoretical loss of three moles of water. At temperatures above 600°C a significant increase in weight loss indicated vaporization of aluminum fluoride. After dehydration a sample of AlF_3 was x-rayed to determine if any hydrolysis had taken place. The x-ray data indicated pure AlF_3 and no significant amount of hydrolysis.

2) Subsolidus Equilibria

The compatability relations at 500°C were determined by studying the subsolidus behavior of selected ternary compositions.

*Allied Chemical Company
**Atomergic Chemetals Company
***Provided by Alcoa Corporation (impurities in weight % are SiO_2 0.14%, KF 0.55%, CaF_2 0.01%, and LiF 0.035%)

All compositions were weighed to $\pm$ 0.1 mg on a Sartorus analytical balance and hand mixed under acetone until near dryness. Each sample was heated in fused silica crucibles in an electrical resistance furnace. After a 48 hour heat treatment at 500°C in air the phases were determined by x-ray diffraction. Due to the slow reaction rates at 500°C most samples were not completely reacted. Each sample was then remixed, reheated, and reexamined until the phases present and relative amounts of each remained constant. At this point the sample was assumed to have reached equilibrium.

3) Liquidus Equilibria

Selected compositions from all areas of the Na_3AlF_6-AlF_3-LiF system were studied to determine the phases in equilibrium on the liquidus surface. Each composition was weighed to 0.1 mg and mixed under acetone until near dryness in the same manner as the subsolidus samples. These compositions were heat treated at 500°C for 16 hours to free the chemically held water from the aluminum fluoride. Several compositions were checked for weight loss to insure no vaporization of aluminum fluoride. Samples of approximately .05 gm were sealed in 3/4 inch lengths of 2 mm diameter platinum tubing by fusing the ends of the tube with a thermocouple welder. Each platinum capsule was then fired in a vertical tube quench furnace*.

* Tem-Pres Research, Inc. State College, Pa.

The temperature in the furnace was controlled to $\pm 3^{\circ}C$ by a Tem-Pres controller. Each capsule was heated to $1000^{\circ}C$ for 30 minutes to insure complete melting and homogeniety. The furnace was cooled to the desired temperature and held for one hour to insure equilibrium before quenching the capsule into cold water. The actual temperature in the furnace was measured using a Pt-Pt/10Rh thermocouple calibrated with several chromel-alumel thermocouples at various temperatures. The sealed tubes were weighed before and after firing to make sure they were airtight. Any tubes that had leaked were discarded and new samples prepared.

All the quenched samples were opened and the contents crushed in an agate mortar and pestel. The crushed material was x-rayed to determine what phases were present. This yielded little useful information because the liquid present at the quenching temperature would often quench into a metastable crystalline phase or a non-equilibrium product. Small amounts of the crushed sample were examined using an optical microscope. From the general appearance it was possible to identify the recrystallized liquid as well as other crystalline phases. The rapidly crystallized liquid appeared as irregular shapes in various sizes that contained many small crystals and many cracks and bubbles. It was often impossible to determine the refractive index of the material because no Becké lines were visible. Crystals that were present at the quenching temperature could be seen as very clear, regular, crystalline shapes. The

refractive index of this material could be found using the Becke' line method. The crystal could then be identified by its refractive index. A change in the refractive index from values reported in the literature would indicate a crystalline solid solution. This did occur in several portions of the diagram. Under the microscope the typical sample would contain one or two crystalline phases plus a varying amount of liquid. Samples were quenched from several temperatures in order to determine the approximate liquidus temperature and the primary phase field to which the composition belonged.

The exact liquidus temperature was verified by running a Differential Thermal Analysis (DTA) on each composition*. Samples run on the DTA were sealed in platinum tubing in the same manner as the previous samples. These tubes were fired at 1000°C for 1/2 hour to insure a homogeneous melt and quenched into cold water. The capsules were again weighed before and after quenching to insure each tube was airtight.

4) Na_3AlF_6-Li_3AlF_6 Diagram

A series of samples at 5% intervals along this join were mixed from Na_3AlF_6, LiF, and AlF_3. They were weighed on a Sartorus analytical balance to 0.1 mg and mixed under acetone. Many of these compositions were run on the DTA. This yielded the approximate

*For description of DTA procedures see page 19

solidus and liquidus temperatures as well as many of the polymorphic inversion temperatures. These experiments did not yield sufficient data to complete the diagram so subsolidus samples were studied at 475, 525, and 575°C. The samples were heated in fused silica crucibles in air at each temperature for 12 hours, remixed, and fired for another 36 hours. The samples were then quenched into cold water and x-rayed to determine the equilibrium phases present.

5) Equipment

a) X-Ray Diffraction

The phases present in each sample were identified by standard x-ray powder diffraction techniques. A Norelco diffractometer with filtered copper radiation, a graphite crystal monochrometer, and pulse height analyser was used for identification. For general phase determination a scan speed of 1°-2θ/minute was used. The precise interplanar spacings of certain solid solutions were measured at a scanning rate of $1/4^{\circ}$-2θ/minute.

b) DTA Equipment

The DTA equipment consisted of a small platinum wound furnace* programmed by an automatic controller**. The samples were heated

*J - 2. R. L. Stone Co., Austin, Texas.
**Controllal, Leeds and Northrup Co., Philadelphia, Pa.

at $8^{\circ}C$/minute but this could be varied by changing cams in the program control unit. The platinum sample containers and standard (calcined Al_2O_3) were placed directly on the Pt-Pt/10Rh thermocouple beads. The differential emf's were recorded versus temperature on an X - Y recorder***.

***Varian Associates, Palo Alto, California.

IV. RESULTS AND DISCUSSION

1) Subsolidus Equilibria*

In order to accurately determine the compatability relations in a ternary system which contains solid solution, it is first necessary to establish the extent of solid solution on all Alkemade lines and then to determine the extent of the associated two phase regions. In the system Na_3AlF_6-AlF_3-LiF there is no appreciable solid solution at 500°C in any of the three boundary systems except for small amounts of solubility of LiF in Na_3AlF_6 and Na_3AlF_6 in LiF. Extensive solid solution of Na_3AlF_6 in Li_3AlF_6 at 500°C is found on the binary join Na_3AlF_6-Li_3AlF_6. Because the exact extent of the solid solution region is prerequisite to determining the phase relations at 500°C, this region was examined by measuring the precise d-spacing of the (220) plane of cryolite, as increasing amounts of Li_3AlF_6 were added. The (220) plane of this crystal was used because it is an intense, isolated peak with a medium large 2θ angle. The precise $d_{(220)}$-spacing for each composition was determined from the average of three measurements taken at a scanning rate of $1/4^{\circ}2\theta$/minute. The ASTM data for pure cryolite gives a value of 1.941 Å which agrees well with 1.942 Å obtained in the present study. The compositions,

*Mr. Richard Baylor, Jr. assisted with the investigation of the subsolidus equilibria at 500°C in this ternary system. The results are scheduled for publication in the Nov. 1974 issue of the Journal of the American Ceramic Society.

heat treatments, and equilibrium phase assemblages used to establish the solid solution limit and the subsolidus relationships are summarized in Table I. The variation of the precise d-spacing, fitted by least squares methods (Appendix A) to a straight line, is shown in Figure 5*. The d-spacing of this plane decreased significantly as lithium cryolite replaced sodium cryolite in the solid solution series. This decrease continued until the d-spacing was 1.929 Å which coincided with the solid solution limit at 500°C of 18 mole % Li_3AlF_6.

Figure 6 shows the phases in equilibrium on the 500°C isothermal section. Seven three-phase regions (compatability triangles) are present, as well as two two-phase regions. The ternary compounds $Na_3Li_3Al_2F_{12}$ and Na_2LiAlF_6 are stable at 500°C and give rise to many of the compatability triangles. The two compatability triangles adjacent to the two-phase regions each contain the limiting cryolite solid solution composition as one of the three compatable phases (i.e. LiF + Na_2LiAlF_6 + $(Na_{0.82}Li_{0.18})_3AlF_6$ and $Na_5Al_3F_{14}$ + Na_2LiAlF_6 + $(Na_{0.82}Li_{0.18})_3AlF_6$). The composition of the cryolite solid solution phase was determined by measuring the $d_{(220)}$-spacing of the phase and noting the corresponding composition from Figure 5. The two-phase regions result from the solid solution region on the lithium cryolite-sodium cryolite join. The two phases in equilibrium in these regions are LiF or $Na_5Al_3F_{14}$ plus a solid solution of Li_3AlF_6

*$d_{(220)}$=1.942 - 0.0007X where X = mole % of Li_3AlF_6

TABLE I

Compositions Used to Determine Compatibility Relations in the System Na_3AlF_6-LiF-AlF_3 at 500°C

Composition (Mole %) Na_3AlF_6	LiF	AlF_3	Firing Time (Hrs)	Phases Present
20	20	60	10	AlF_3 $Na_3Li_3Al_2F_{12}$ $Na_5Al_3F_{14}$
10	50	40	10	AlF_3 $Na_3Li_3Al_2F_{12}$ β-Li_3AlF_6
5	80	15	24	LiF $Na_3Li_3Al_2F_{12}$
33	42	25	64	$Na_5Al_3F_{14}$ $Na_3Li_3Al_2F_{12}$ α-Na_2LiAlF_6
20	65	15	64	LiF $Na_3Li_3Al_2F_{12}$ α-Na_2LiAlF_6
50	25	25	64	$Na_5Al_3F_{14}$ α-Na_2LiAlF_6 α-$Na_3AlF_{6_{ss}}$ (18%Li_3AlF_6)
30	60	10	112	LiF α-Na_2LiAlF_6 α-$Na_3AlF_{6_{ss}}$ (18%Li_3AlF_6)
70	15	15	72	$Na_5Al_3F_{14}$ α-$Na_3AlF_{6_{ss}}$ (8%Li_3AlF_6)

TABLE I (Cont'd)

Compositions Used to Determine Compatibility Relations in the System Na_3AlF_6-LiF-AlF_3 at 500°C

Composition (Mole %) Na_3AlF_6	LiF	AlF_3	Firing Time (Hrs)	Phases Present
85	13	2	72	LiF α-$Na_3AlF_{6_{ss}}$ (4%Li_3AlF_6)
33.4	50	16.6	120	α-Na_2LiAlF_6 α-$Na_3AlF_{6_{ss}}$ (18%Li_3AlF_6)(TR)
45	41.4	13.6	48	α-Na_2LiAlF_6 α-$Na_3AlF_{6_{ss}}$ (18%Li_3AlF_6)
55	33.8	11.2	120	α-Na_2LiAlF_6 (TR) α-Na_3AlF_6 (17%Li_3AlF_6)
65	26.3	8.7	72	α-$Na_3AlF_{6_{ss}}$ (12.5%Li_3AlF_6)
75	18.8	6.2	72	α-$Na_3AlF_{6_{ss}}$ (7.4%Li_3AlF_6)
85	11.4	3.6	72	α-$Na_3AlF_{6_{ss}}$ (4.4%Li_3AlF_6)

(TR) - Trace

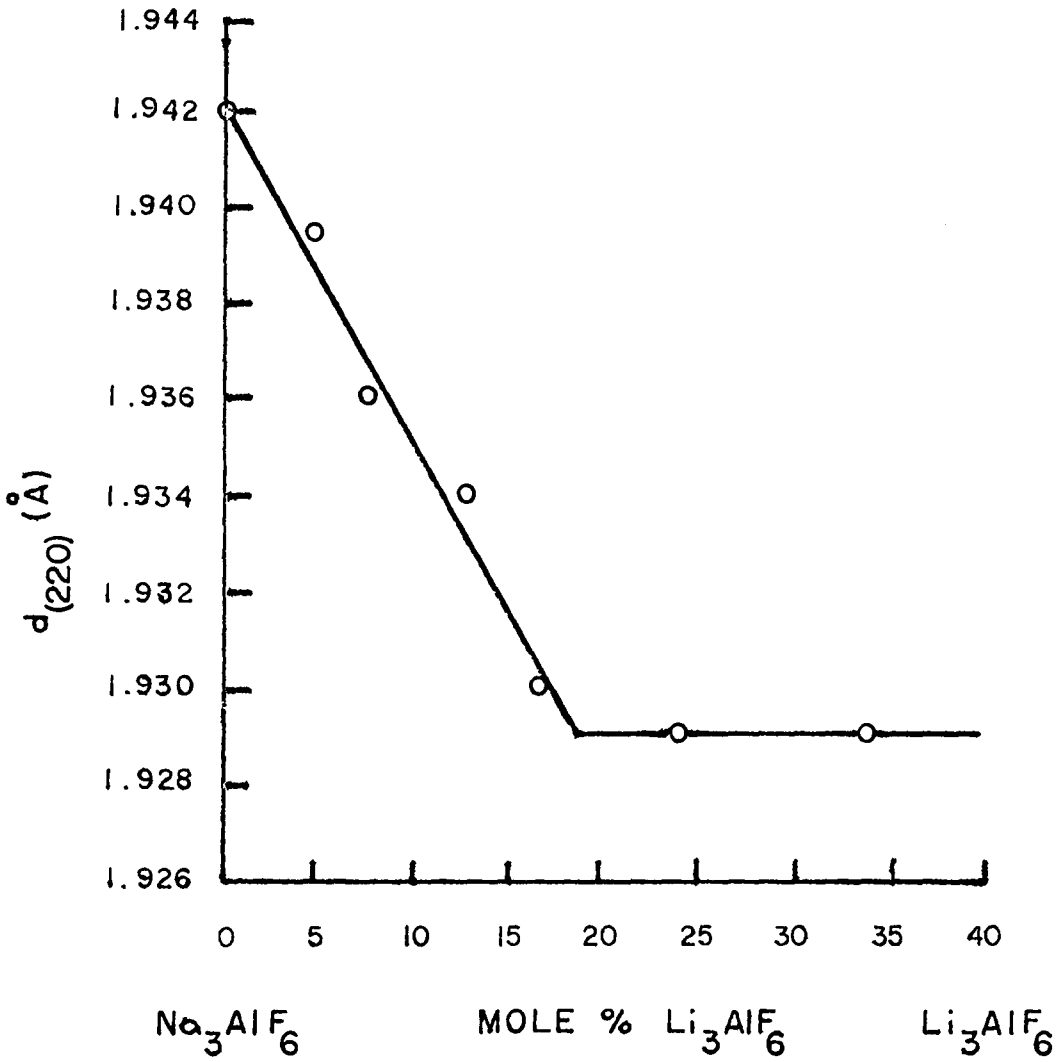

FIGURE 5. PRECISION d SPACING OF 220 PLANE IN A SOLID SOLUTION OF Li_3AlF_6 IN Na_3AlF_6

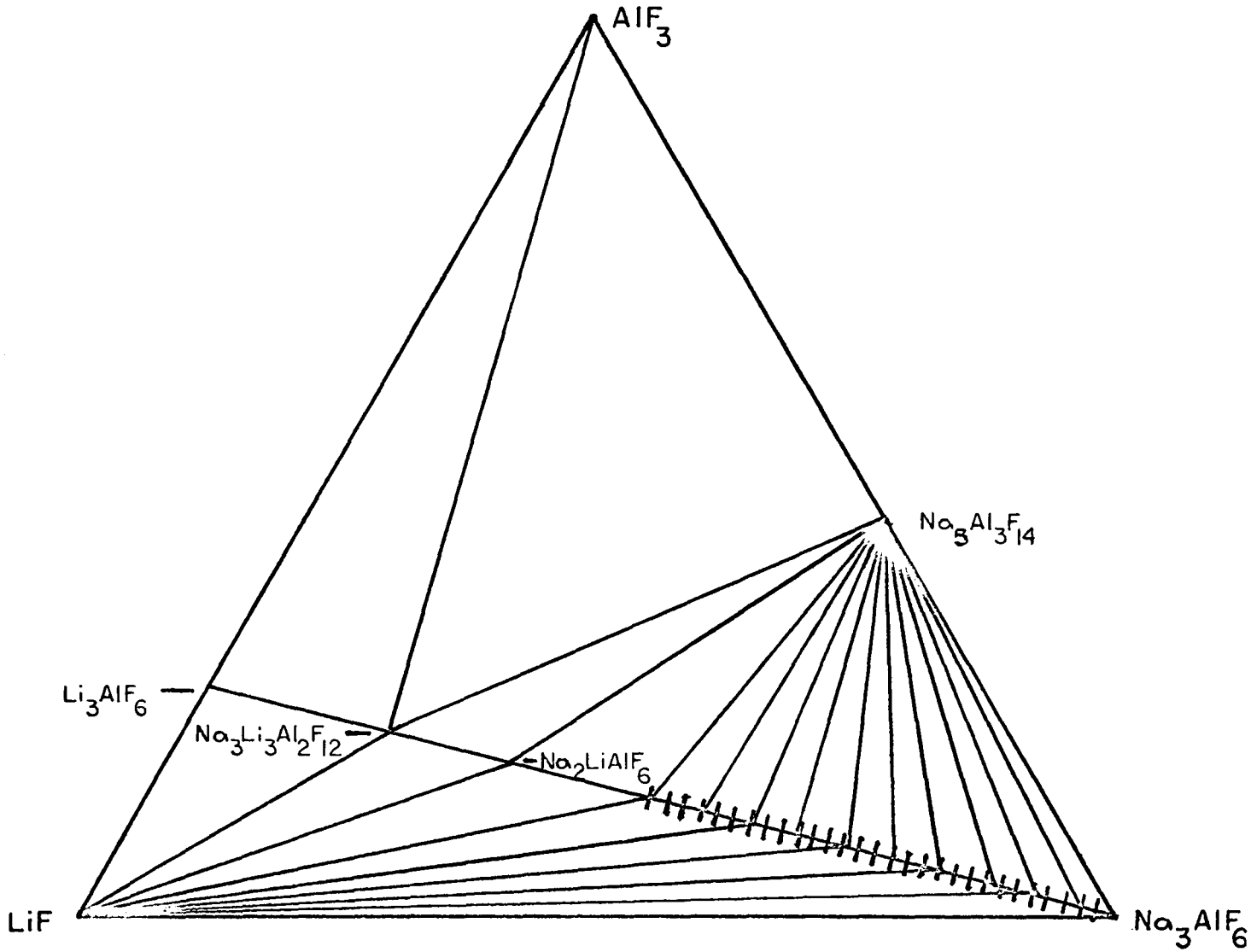

FIGURE 6. COMPATIBILITY RELATIONS AT 500 °C IN THE SYSTEM Na_3AlF_6 - LiF - AlF_3

in Na_3AlF_6. Liquid was not observed anywhere in the ternary system at 500°C.

Below 500°C the phase relations are essentially the same as those observed at 500°C. At 420°C, β-Na_2LiAlF_6 inverts to the low temperature α form. As temperature decreases, the extent of solubility of Li_3AlF_6 in Na_3AlF_6 decreases; consequently, the two-phase regions in Figure 6 will decrease in size and the adjoining three-phase regions will progressively expand towards the pure cryolite composition. Reaction rates were found to become prohibitively slow at 400°C and below, making it impossible to obtain equilibrium in any reasonable time.

2) Liquidus

The compositions investigated and equilibrium phases present at high temperatures are shown in Table II. Each composition was heat treated, quenched and examined under the optical microscope. The optical examination consisted of determining what crystals were present by measuring the average refractive index of each crystal using oils of known refractive indices and following the Becke' line method.

In the lithium fluoride rich side of the diagram the LiF phase field proved easy to locate. When compositions inside the LiF primary phase field were examined rounded crystals with a refractive index of 1.39 were observed. When this boundary was crossed

TABLE II

Compositions Used to Determine the Liquidus Relations in the System Na_3AlF_6-AlF_3-LiF

Composition (Mole %) Na_3AlF_6	LiF	AlF_3	Primary Phase As Seen Using An Optical Microscope
5.0	75.0	20.0	Li_3AlF_6
5.0	77.5	17.5	Li_3AlF_6
5.0	80.0	15.0	Li_3AlF_6
5.0	82.5	12.5	Li_3AlF_6
5.0	85.0	10.0	LiF
10.0	85.0	5.0	LiF
12.5	82.5	5.0	Na_3AlF_{6ss}
15.0	80.0	5.0	Na_3AlF_{6ss}
17.5	77.5	5.0	Na_3AlF_{6ss}
20.0	75.0	5.0	Na_3AlF_{6ss}
7.5	85.0	7.5	LiF
8.75	82.5	8.75	LiF
10.0	80.0	10.0	Na_3AlF_{6ss}
11.25	77.5	11.25	Na_3AlF_{6ss}
12.5	75.0	12.5	Na_3AlF_{6ss}
10.0	75.0	15.0	Li_3AlF_6
7.5	75.0	17.5	Li_3AlF_6
7.5	80.0	12.5	Li_3AlF_6

TABLE II (Cont'd)

Compositions Used to Determine the Liquidus Relations in the System Na_3AlF_6-AlF_3-LiF

Composition (Mole %) Na_3AlF_6	LiF	AlF_3	Primary Phase As Seen Using An Optical Microscope
25.0	20.0	55.0	AlF_3
30.0	20.0	50.0	$Na_5Al_3F_{14}$
35.0	20.0	45.0	$Na_5Al_3F_{14}$
40.0	20.0	40.0	$Na_5Al_3F_{14}$
45.0	20.0	35.0	Na_3AlF_{6ss}
15.0	35.0	50.0	AlF_3
20.0	35.0	45.0	$Na_5Al_3F_{14}$
25.0	35.0	40.0	$Na_5Al_3F_{14}$
30.0	35.0	35.0	$Na_5Al_3F_{14}$
35.0	35.0	30.0	Na_3AlF_{6ss}
10.0	45.0	45.0	AlF_3
15.0	45.0	40.0	$Na_3Li_3Al_2F_{12}$
20.0	45.0	35.0	$Na_3Li_3Al_2F_{12}$
25.0	45.0	30.0	$Na_3Li_3Al_2F_{12}$
30.0	45.0	25.0	Na_3AlF_{6ss}
10.0	50.0	40.0	AlF_3
15.0	50.0	35.0	$Na_3Li_3Al_2F_{12}$
20.0	50.0	30.0	$Na_3Li_3Al_2F_{12}$
25.0	50.0	25.0	Na_3AlF_{6ss}

TABLE II (Cont'd)

Compositions Used to Determine the Liquidus Relations in the System Na_3AlF_6-AlF_3-LiF

Composition (Mole %) Na_3AlF_6	LiF	AlF_3	Primary Phase As Seen Using An Optical Microscope
10.0	55.0	35.0	$Na_3Li_3Al_2F_{12}$
15.0	55.0	30.0	$Na_3Li_3Al_2F_{12}$
20.0	55.0	25.0	Na_3AlF_{6ss}
10.0	60.0	30.0	$Na_3Li_3Al_2F_{12}$
7.5	65.0	27.5	AlF_3
7.5	62.5	30.0	AlF_3
7.5	60.0	32.5	$Na_3Li_3Al_2F_{12}$
7.5	57.5	35.0	$Na_3Li_3Al_2F_{12}$
7.5	55.0	37.5	Li_3AlF_6
7.5	52.5	40.0	Li_3AlF_6
7.5	50.0	42.5	Li_3AlF_6
4.0	56.0	40.0	AlF_3
4.0	58.5	37.5	Li_3AlF_6
4.0	61.0	35.0	Li_3AlF_6
4.0	63.5	32.5	Li_3AlF_6
4.0	66.0	30.0	Li_3AlF_6
5.0	70.0	25.0	Li_3AlF_6
2.5	67.5	25.0	Li_3AlF_6
10.0	65.5	25.0	Na_3AlF_{6ss}
12.5	60.0	25.0	Na_3AlF_{6ss}

the crystals of Li_3AlF_6 or Na_3AlF_6 were noticeably more angular and had a lower refractive index. The boundary between Li_3AlF_6 and Na_3AlF_6 was very difficult to locate. The refractive indices of pure monoclinic Na_3AlF_6 are α=1.339, β=1.339, γ=1.340 and those of Li_3AlF_6 are ϵ=1.373 and ω=1.374. The refractive indices of both crystals changed significantly due to extensive solid solution. The refractive index of Li_3AlF_6 decreased from 1.373 to 1.370 as more and more Na_3AlF_6 went into solution in Li_3AlF_6. Na_3AlF_6 underwent a much more drastic change in refractive index. It increased from 1.340 to 1.360 as Li_3AlF_6 dissolved in Na_3AlF_6. This made the boundary between Li_3AlF_6 and Na_3AlF_6 impossible to determine using the Becke' line method. Scanning electron micrographs of both crystals were examined to see if the boundary could be identified using cleavage, shape, or any other noticeable surface feature. Unfortunately the crystals looked so much alike no boundary could be detected by this method; the boundary was later found using results from the DTA.

The phase boundary between AlF_3 and $Na_5Al_3F_{14}$ was not difficult to determine. The refractive indices of AlF_3 (ϵ=1.377, ω=1.3765) and $Na_5Al_3F_{14}$ (ϵ=1.3424, ω=1.349) were sufficiently different to enable determination of the boundary. X-ray examinations in this portion of the diagram were also helpful because samples quenched from above the liquidus in this portion of the diagram crystallized into metastable $Na_5Al_3F_{14}$. Quenched samples anywhere in the area (regardless of what primary phase field) showed a diffraction pattern

of $Na_5Al_3F_{14}$. Compositions quenched from below the liquidus showed diffraction patterns of the primary crystals and metastable $Na_5Al_3F_{14}$. A sample quenched from below the liquidus in the AlF_3 phase field showed a trace of AlF_3 present on the diffraction pattern along with $Na_5Al_3F_{14}$ from the metastable recrystallized liquid. In the $Na_5Al_3F_{14}$ phase field diffraction patterns showed only $Na_5Al_3F_{14}$ from both the primary crystals and the metastable $Na_5Al_3F_{14}$. The adjacent boundary between $Na_5Al_3F_{14}$ and Na_3AlF_6 was found in a like manner using refractive indices and x-ray diffraction data.

The boundary between AlF_3 and either Li_3AlF_6 or $Na_3Li_3Al_2F_{12}$ was possibly the easiest to determine. AlF_3 crystals in this portion of the primary phase field were very nearly opaque. The difference in crystal appearance in the AlF_3 phase field indicates solid solution. The opaque crystals were easily distinguished from angular, clear Li_3AlF_6 or $Na_3Li_3Al_2F_{12}$ crystals. The boundary between Li_3AlF_6 and $Na_3Li_3Al_2F_{12}$ was distinguishable because the cubic $Na_3Li_3Al_2F_{12}$ crystals had a lower refractive index (1.340) than Li_3AlF_6.

The boundary between $Na_3Li_3Al_2F_{12}$ and Na_3AlF_6 was found by identifying the phases through measuring the refractive indices of the primary crystals. The boundary between $Na_5Al_3F_{14}$ and $Na_3Li_3Al_2F_{12}$ was not distinguishable using this method, but the boundary could be located by observing that the tetragonal $Na_5Al_3F_{14}$ crystals showed an extinction position under the microscope while the cubic $Na_3Li_3Al_2F_{12}$ crystals did not.

To verify the phase boundaries and determine the exact liquidus temperature, each composition was sealed in platinum capsules and run on the DTA. The DTA results show the liquidus and solidus temperatures very clearly along with several polymorphic transformations. Figures 7 and 8 show two typical DTA patterns. Figure 7 shows the DTA pattern of pure cryolite. The peak observed is the polymorphic transformation of monoclinic β cryolite to cubic α cryolite. This DTA pattern was not run to a high enough temperature to observe the liquidus peak. Figure 8 shows a ternary composition within the Li_3AlF_6 primary phase field. This pattern shows a small peak at about 500°C where the β polymorph transforms to γ. At 600°C there is another polymorphic inversion of the γ form to the δ form. The last two peaks show the eutectic temperature at 690°C and the liquidus temperature of 715°C.

Figure 9 shows the proposed phase diagram for the Na_3AlF_6-AlF_3-LiF system. This was determined using the DTA results shown in Figures 10 and 11 and the microscopic results listed in Table II. There are seven primary phase fields present on the liquidus surface. The dotted boundary (isotherm) indicates the transformation of α'-Na_3AlF_6 to α-Na_3AlF_6. It should be noted that the ternary compound Na_2LiAlF_6 decomposes at a temperature well below the liquidus and that the ternary compound $Na_3Li_3Al_2F_{12}$ decomposes at the temperature of the reaction point.

The liquidus surface in the Na_3AlF_6-Li_3AlF_6-LiF portion of the

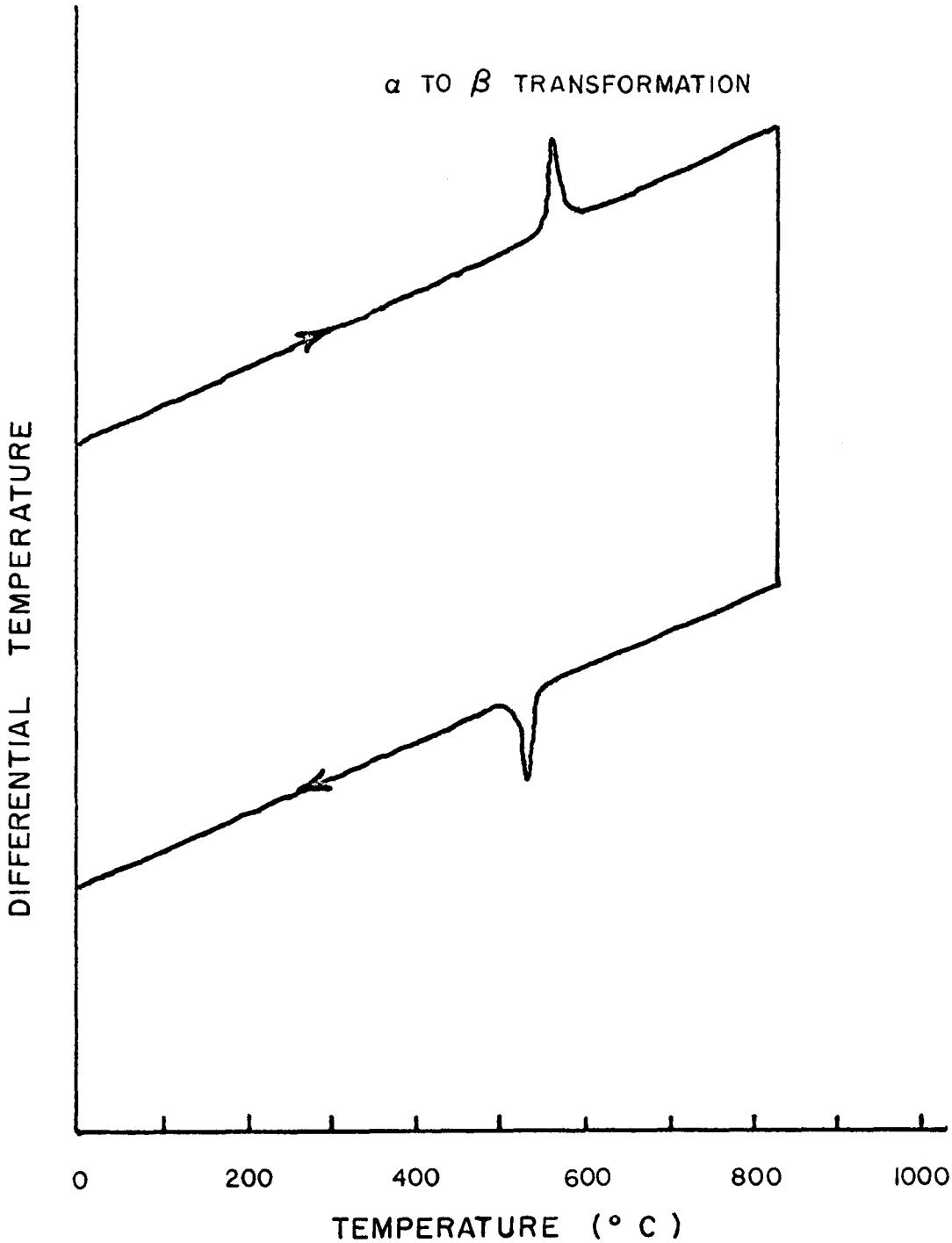

FIGURE 7. DTA PATTERN FOR PURE Na_3AlF_6

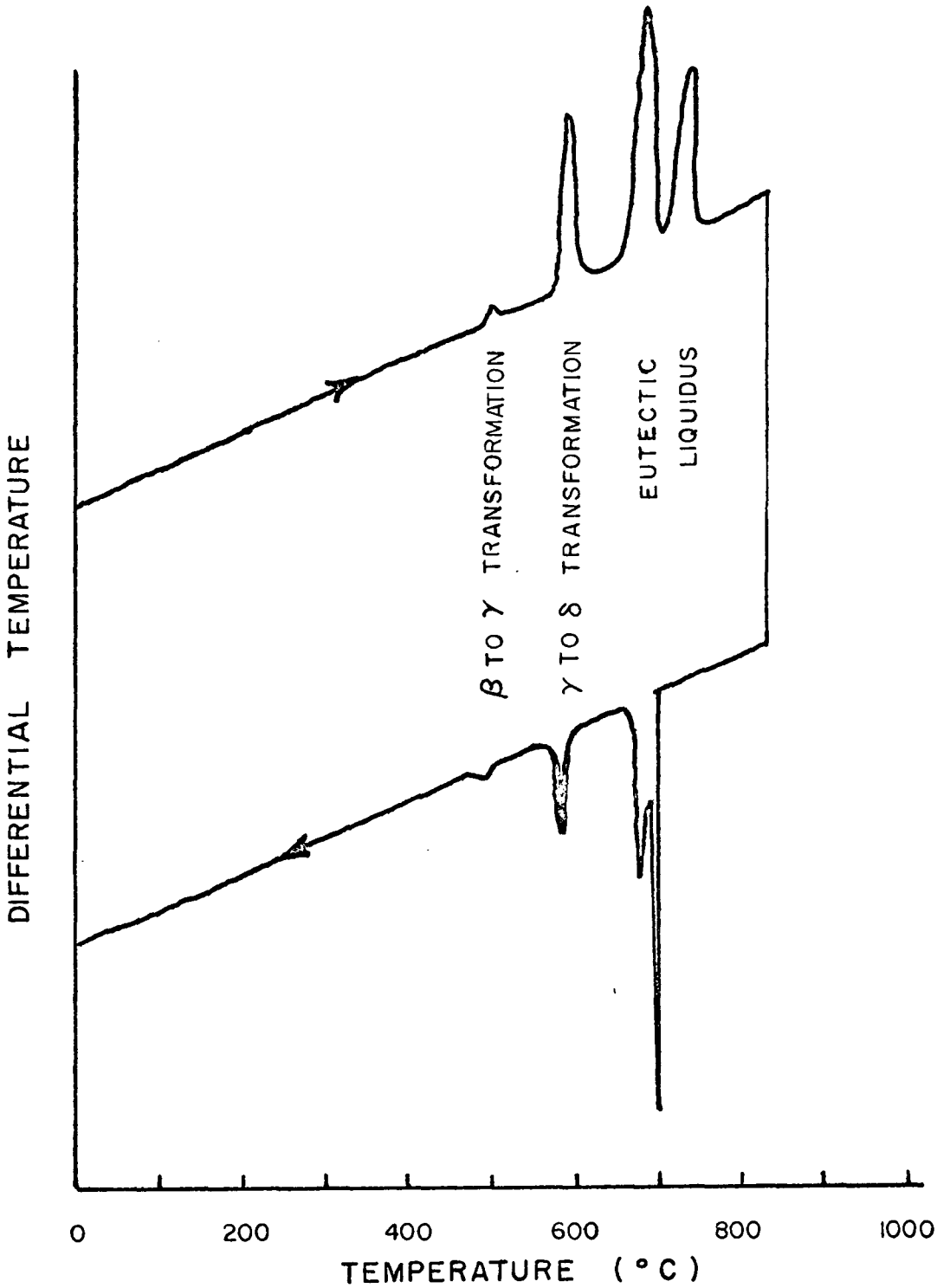

FIGURE 8. DTA PATTERN FOR A COMPOSITION FROM Li_3AlF_6 PHASE FIELD

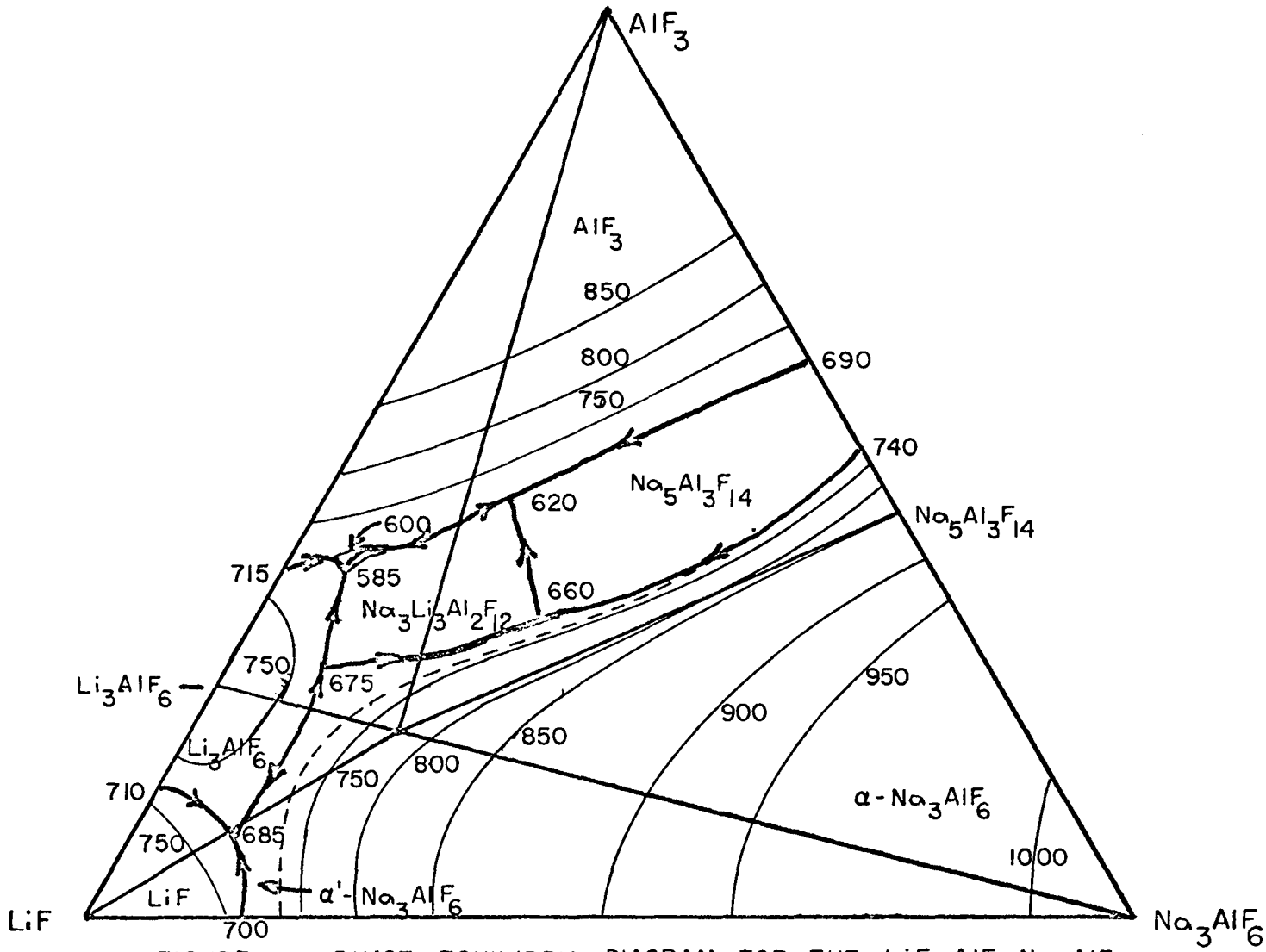

FIGURE 9. PHASE EQUILIBRIA DIAGRAM FOR THE $LiF-AlF_3-Na_3AlF_6$ TERNARY SYSTEM SHOWING LIQUIDUS SURFACE FEATURES

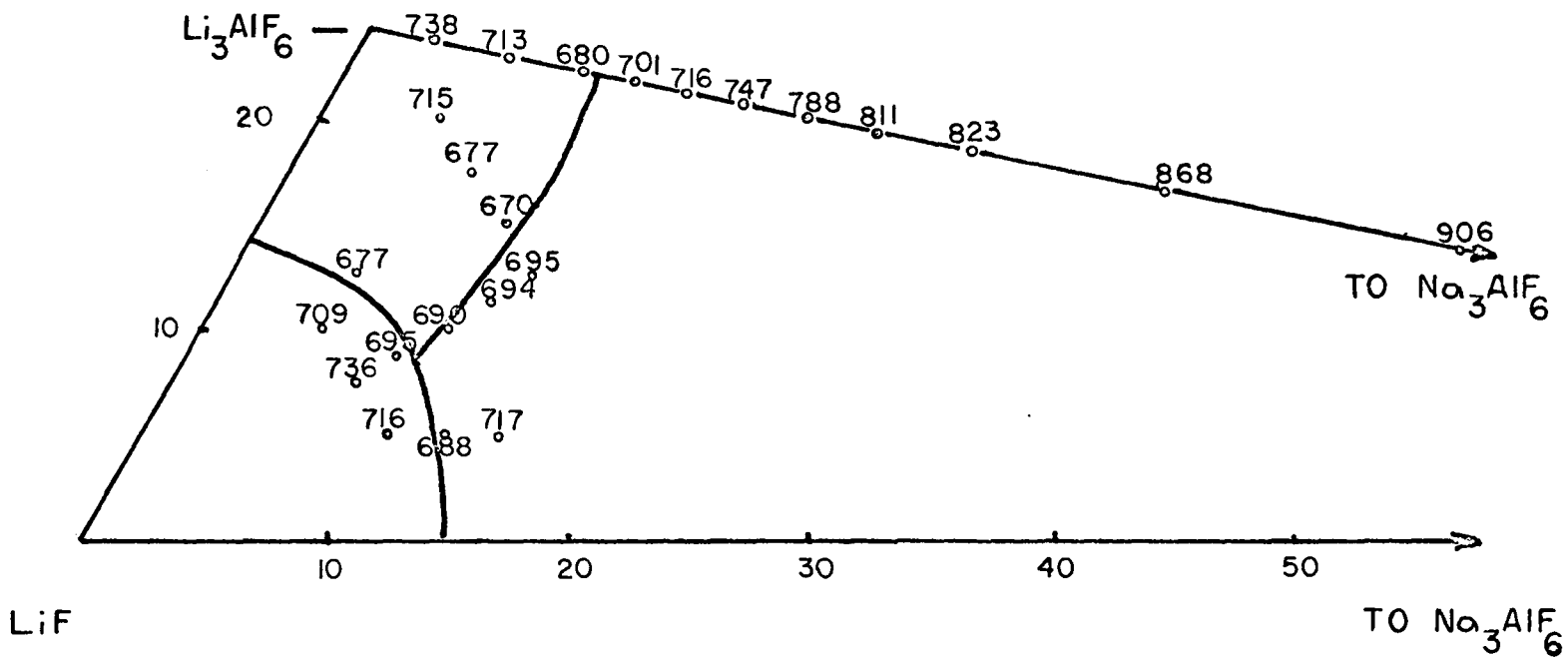

FIGURE 10. LIQUIDUS TEMPERATURES IN A PORTION OF THE LiF-Li_3AlF_6-Na_3AlF_6 SYSTEM AS DETERMINED BY DTA

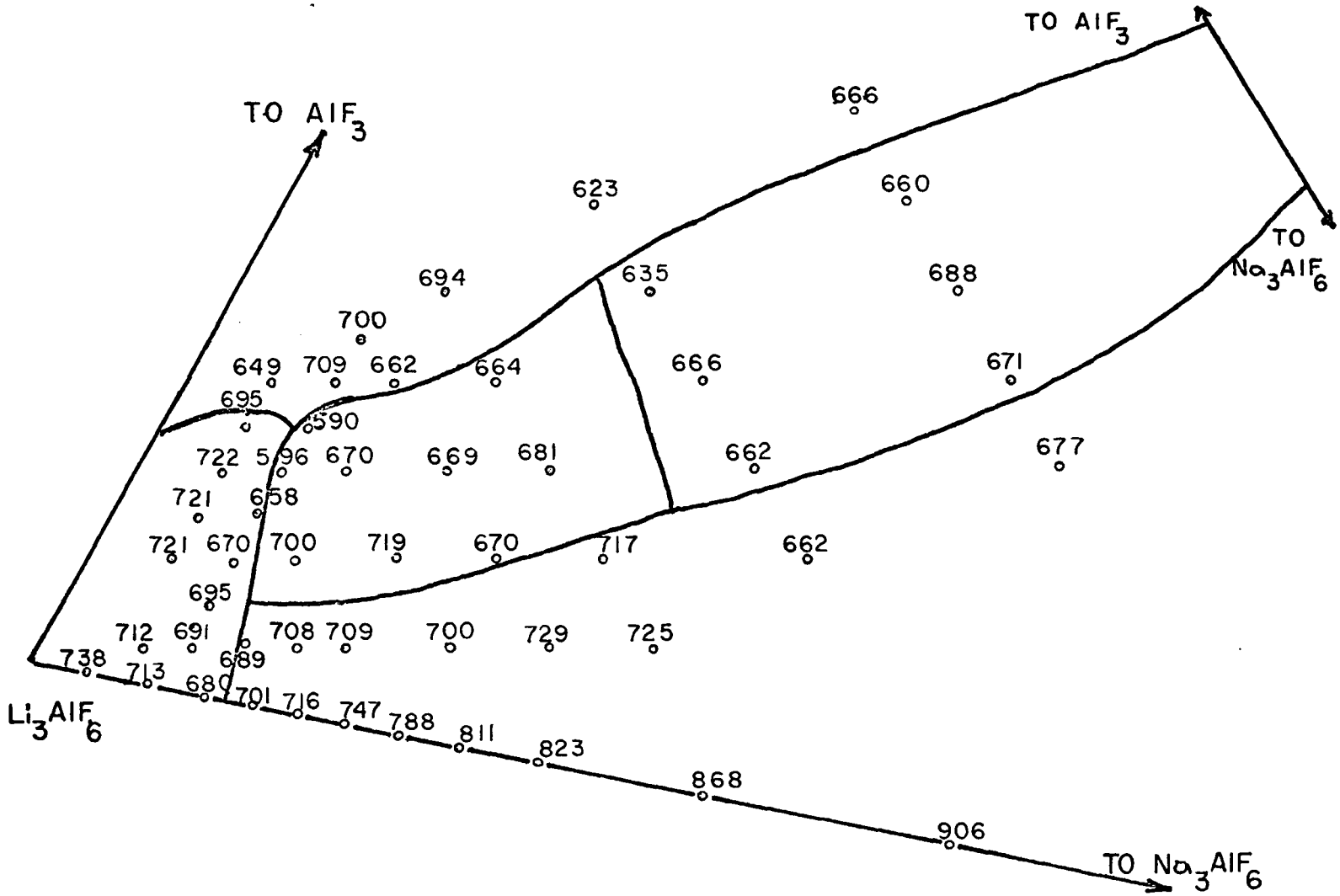

FIGURE 11. LIQUIDUS TEMPERATURES IN A PORTION OF THE Li_3AlF_6 - AlF_3 - Na_3AlF_6 SYSTEM AS DETERMINED BY DTA

diagram contains a ternary eutectic. Two of the boundary curves which meet to form this eutectic start at binary eutectics and slope gradually to the ternary eutectic located at 685 ± 5°C and 81% LiF, 9.5% Na_3AlF_6, and 9.5% AlF_3. The final boundary curve leading to this eutectic originates at the saddle point on the Na_3AlF_6-Li_3AlF_6 join.

The Li_3AlF_6-Na_3AlF_6-AlF_3 portion of the ternary system contains a reaction point, a ternary peritectic, and two ternary eutectics. The boundary curve between the Li_3AlF_6 and Na_3AlF_6 phase fields slope to the reaction point from the saddle point on the Na_3AlF_6-Li_3AlF_6 join. The reaction point exists at 65% LiF, 9% Na_3AlF_6, and 26% AlF_3 and signifies the decomposition of $Na_3Li_3Al_2F_{12}$ at 675°C. The boundary curves slope downward in two directions from this reaction point. The slope is very steep when following the boundary between Li_3AlF_6 and $Na_3Li_3Al_2F_{12}$ and continuing to the ternary eutectic at 585 ± 5°C. This eutectic joins the phase fields of AlF_3, Li_3AlF_6, and $Na_3Li_3Al_2F_{12}$ and lies at a composition of 56% LiF, 6% Na_3AlF_6, and 38% AlF_3. The other boundary curves which terminate at this eutectic originate at the binary eutectic between Li_3AlF_6 and AlF_3, and the saddle point that lies on the AlF_3-$Na_3Li_3Al_2F_{12}$ join.

The boundary curve separating the phase fields of $Na_3Li_3Al_2F_{12}$ and Na_3AlF_6 starts at the reaction point and decreases very slowly to the ternary peritectic at 660 ± 5°C. This peritectic has the composition of 30% LiF, 37% Na_3AlF_6, and 33% AlF_3. The other boundary

curve sloping downward to the peritectic starts at the binary peritectic on the AlF_3-Na_3AlF_6 join. The final ternary eutectic connects the phase fields of AlF_3, $Na_5Al_3F_{14}$, and $Na_3Li_3Al_2F_{12}$ and occurs at 620 $\pm$ 5°C and 46% AlF_3, 17% Na_3AlF_6, and 37% LiF. The boundary curves descending on this ternary eutectic originate at the ternary peritectic, the $Na_3Li_3Al_2F_{12}$-AlF_3 saddle point, and the AlF_3-Na_3AlF_6 binary eutectic.

3) The Na_3AlF_6-Li_3AlF_6

The binary system Na_3AlF_6 -Li_3AlF_6 lies in the center of the ternary system discussed above. This true binary join was reexamined because the existing version of this equilibrium diagram does not agree with the liquidus surface determined in this study. The proposed binary diagram as determined by DTA and subsolidus heat treatments is shown in Figure 12.

The first feature to note about this system is the high temperature behavior of the compound Na_2LiAlF_6. It behaves as a stable stoichiometric compound up to 510°C where it decomposes to the intermediate solid solution α'-$Na_3AlF_{6(ss)}$ and α-$Na_3AlF_{6(ss)}$. This was determined from DTA results shown in Figure 12 as well as subsolidus heat treatments and results shown in Table III. Subsolidus results at 475°C show the solid solution of Li_3AlF_6 in Na_3AlF_6 to exist to somewhere between 15 and 20% Li_3AlF_6 which agrees with Figure 5. At 525 and 575°C the solid solution exists over to 40%

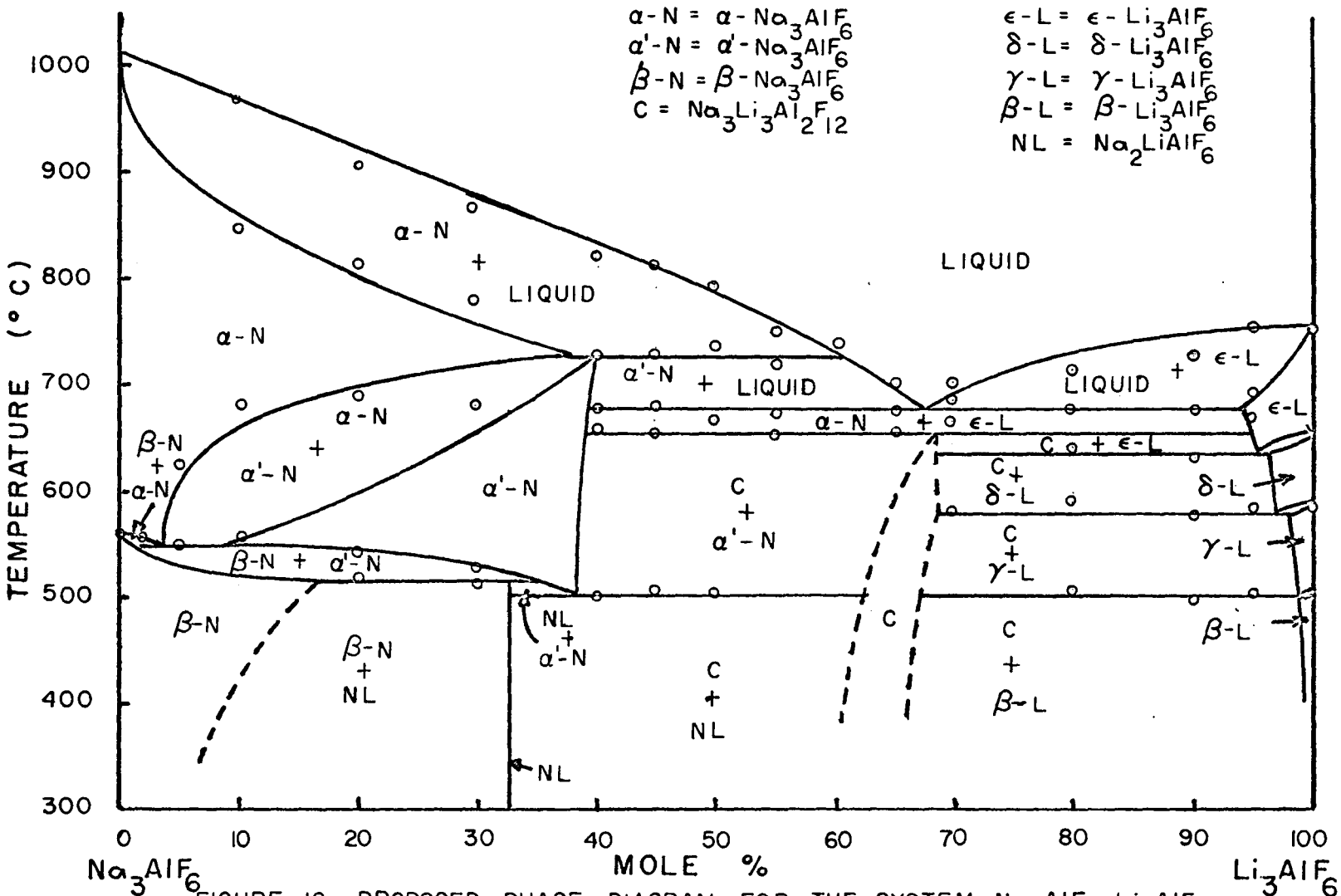

FIGURE 12. PROPOSED PHASE DIAGRAM FOR THE SYSTEM Na_3AlF_6 - Li_3AlF_6
(CIRCLES INDICATE DTA PEAKS)

TABLE III

Compositions, Heat Treatments, and Phase Assemblages Used to Determine the Phase Relations on the Na_3AlF_6-Li_3AlF_6 Join.

Composition (mole %)		475	525	575
Na_3AlF_6	Li_3AlF_6			
95	5	Na_3AlF_6	Na_3AlF_6	Na_3AlF_6
90	10	Na_3AlF_6	Na_3AlF_6	Na_3AlF_6
85	15	Na_3AlF_6	Na_3AlF_6	Na_3AlF_6
80	20	Na_3AlF_6 Na_2LiAlF_6	Na_3AlF_6	Na_3AlF_6
75	25	Na_3AlF_6 Na_2LiAlF_6	Na_3AlF_6 Na_2LiAlF_6	Na_3AlF_6
70	30	Na_3AlF_6 Na_2LiAlF_6 $Na_3Li_3Al_2F_{12}$	Na_3AlF_6 Na_2LiAlF_6	Na_3AlF_6
65	35	tr Na_3AlF_6 Na_2LiAlF_6 $Na_3Li_3Al_2F_{12}$	Na_3AlF_6 Na_2LiAlF_6	Na_3AlF_6
60	40	Na_2LiAlF_6 $Na_3Li_3Al_2F_{12}$	Na_3AlF_6 Na_2LiAlF_6	Na_3AlF_6
55	45	Na_2LiAlF_6 $Na_3Li_3Al_2F_{12}$	Na_2LiAlF_6 $Na_3Li_3Al_2F_{12}$	Na_3AlF_6
50	50	Na_2LiAlF_6 $Na_3Li_3Al_2F_{12}$	Na_2LiAlF_6 $Na_3Li_3Al_2F_{12}$	Na_2LiAlF_6 $Na_3Li_3Al_2F_{12}$
45	55	Na_2LiAlF_6 $Na_3Li_3Al_2F_{12}$	Na_2LiAlF_6 $Na_3Li_3Al_2F_{12}$	Na_2LiAlF_6 $Na_3Li_3Al_2F_{12}$

TABLE III (cont'd)

Compositions, Heat Treatments, and Phase Assemblages Used to Determine the Phase Relations on the Na_3AlF_6-Li_3AlF_6 Join.

Composition (mole %)		475	525	575
Na_3AlF_6	Li_3AlF_6			
40	60	Na_2LiAlF_6 $Na_3Li_3Al_2F_{12}$	Na_2LiAlF_6 $Na_3Li_3Al_2F_{12}$	Na_2LiAlF_6 $Na_3Li_3Al_2F_{12}$
35	65	tr Li_3AlF_6 tr Na_2LiAlF_6 $Na_3Li_3Al_2F_{12}$	Na_2LiAlF_6 $Na_3Li_3Al_2F_{12}$	Unidentifiable
30	70	Li_3AlF_6 $Na_3Li_3Al_2F_{12}$	tr Li_3AlF_6 tr Na_2LiAlF_6 $Na_3Li_3Al_2F_{12}$	Unidentifiable
25	75	Li_3AlF_6 $Na_3Li_3Al_2F_{12}$	Li_3AlF_6 $Na_3Li_3Al_2F_{12}$	Unidentifiable
20	80	Li_3AlF_6 $Na_3Li_3Al_2F_{12}$	Li_3AlF_6 $Na_3Li_3Al_2F_{12}$	Unidentifiable
15	85	Li_3AlF_6 $Na_3Li_3Al_2F_{12}$	Li_3AlF_6 $Na_3Li_3Al_2F_{12}$	Unidentifiable
10	90	Li_3AlF_6 $Na_3Li_3Al_2F_{12}$	Li_3AlF_6 $Na_3Li_3Al_2F_{12}$	Unidentifiable
5	95	Li_3AlF_6 $Na_3Li_3Al_2F_{12}$	Li_3AlF_6 $Na_3Li_3Al_2F_{12}$	Unidentifiable

Li_3AlF_6. The solid solution is present because α'-Na_3AlF_6 has formed but on quenching has transformed to the low temperature β polymorph. Garton and Wanklyn[15] have reported a similar phase field for α'-Na_3AlF_6.

The compound $Na_3Li_3Al_2F_{12}$ also has interesting high temperature behavior. It is not a stoichiometric compound but exists as a narrow solid solution region. Subsolidus results show this compound to exist between 35 and 40% Na_3AlF_6. This region is unclear because quenching in this portion of the diagram yields non-equilibrium phases, either too many phases present or unidentifiable phases present on the diffraction patterns. The DTA results show the $Na_3Li_3Al_2F_{12}$ solid solution to exist up to 670 $\pm$ 5°C where it decomposes to $Na_3AlF_{6(ss)}$ + Li_3AlF_6. Garton and Wanklyn also agree with this behavior of $Na_3Li_3Al_2F_{12}$. They show a solid solution between 40 and 45% Na_3AlF_6 existing up to approximately 680°C.

The eutectoid at 4% Li_3AlF_6 and 552°C was found using DTA results of compositions run at 0, 2, 5, and 10% Li_3AlF_6. The heating curves from these DTA's are compared in Figure 13. The 10% composition shows the heat effects for the eutectoid at 552°C and the boundary between ($\alpha'Na_3AlF_6$ + α-Na_3AlF_6) and α-Na_3AlF_6. The 5% composition shows these same two peaks but they are much closer together. When the 2% sample was run the DTA showed only one peak indicating that the eutectoid was at a higher % Li_3AlF_6. Pure Na_3AlF_6 showed one peak at a temperature which agreed with the

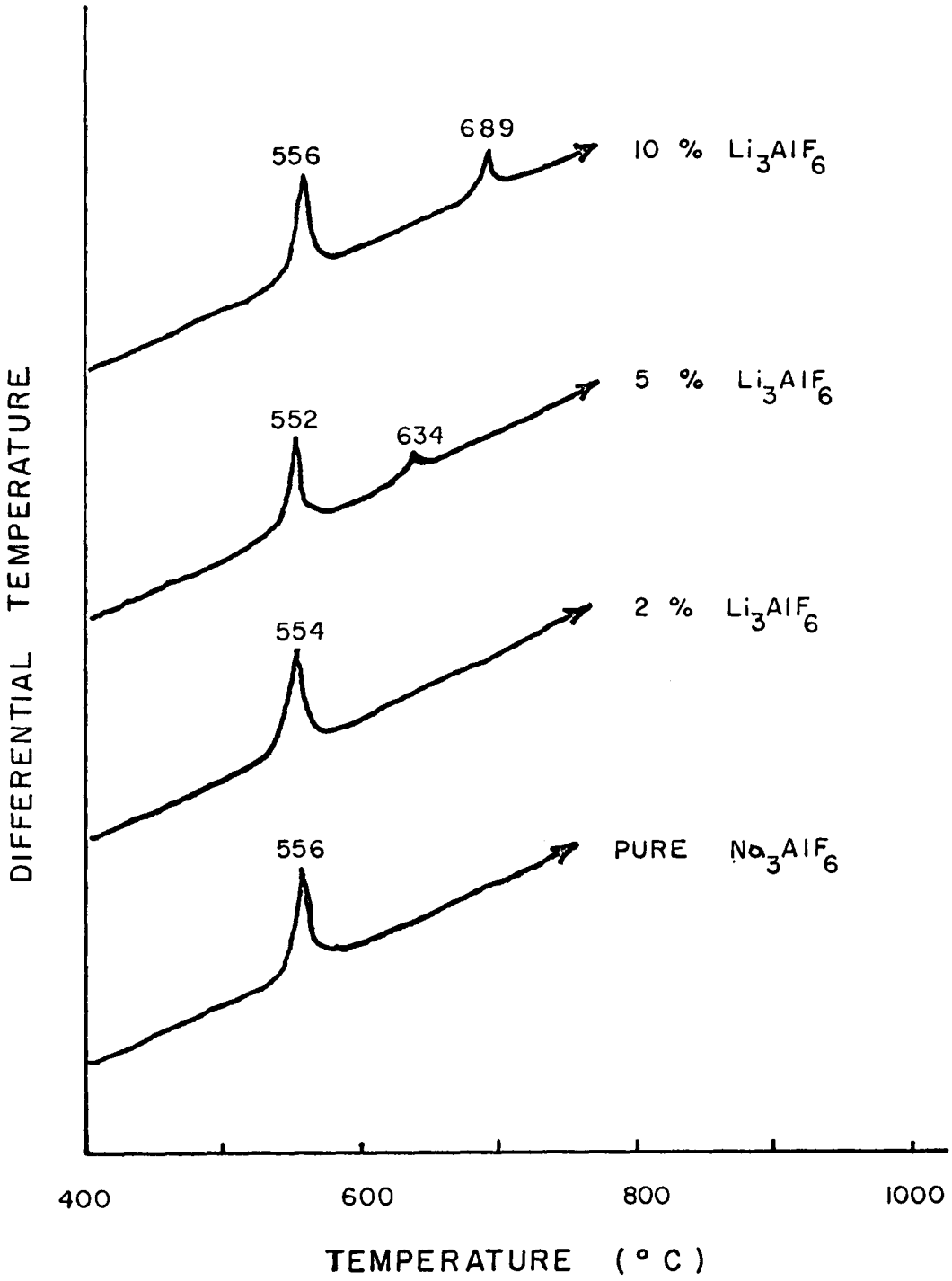

FIGURE 13. COMPARISON OF DTA PEAKS OF Na_3AlF_6 RICH COMPOSITIONS

transformation temperature reported in the literature. The phases in equilibrium at this eutectoid are β-$Na_3AlF_{6(ss)}$ plus an intermediate solid solution α'-$Na_3AlF_{6(ss)}$.

The portion of the diagram from 90% Li_3AlF_6 to pure Li_3AlF_6 was determined using the DTA results shown in Figure 14. The peak near 500°C on all three patterns is due to the polymorphic inversion at 510°C. The temperature of this peak decreases as Na_3AlF_6 is added. This decrease is only 1 or 2 degrees and the temperature has stabilized by 5% Na_3AlF_6 suggesting little solid solution. The peak at 570°C for Li_3AlF_6 is caused by a polymorphic inversion usually seen at 597°C. This peak has decreased to 554°C for the 5 and 10% Na_3AlF_6 compositions suggesting small amounts of solid solution existing to about 3% Na_3AlF_6. This gives rise to a eutectoid reaction isotherm at 554°C. Two DTA peaks occur between 630°C and 680°C for these compositions. The small lower temperature peak is due to the polymorphic inversion from δ to ϵ-Li_3AlF_6 and the large peak is due to the eutectic reaction. The presence of a large eutectic peak on the curve labeled Li_3AlF_6 indicates the composition was not pure. Other indications of this are the low melting point and the low δ to ϵ inversion temperature. Pure Li_3AlF_6 should show only a small peak near 680°C where δ-Li_3AlF_6 transforms to ϵ-Li_3AlF_6. The small peak for the Li_3AlF_6 composition is obscured by the eutectic peak. The decreasing temperature of the polymorphic inversion indicates a significant solid solution region extending to about 5% Na_3AlF_6.

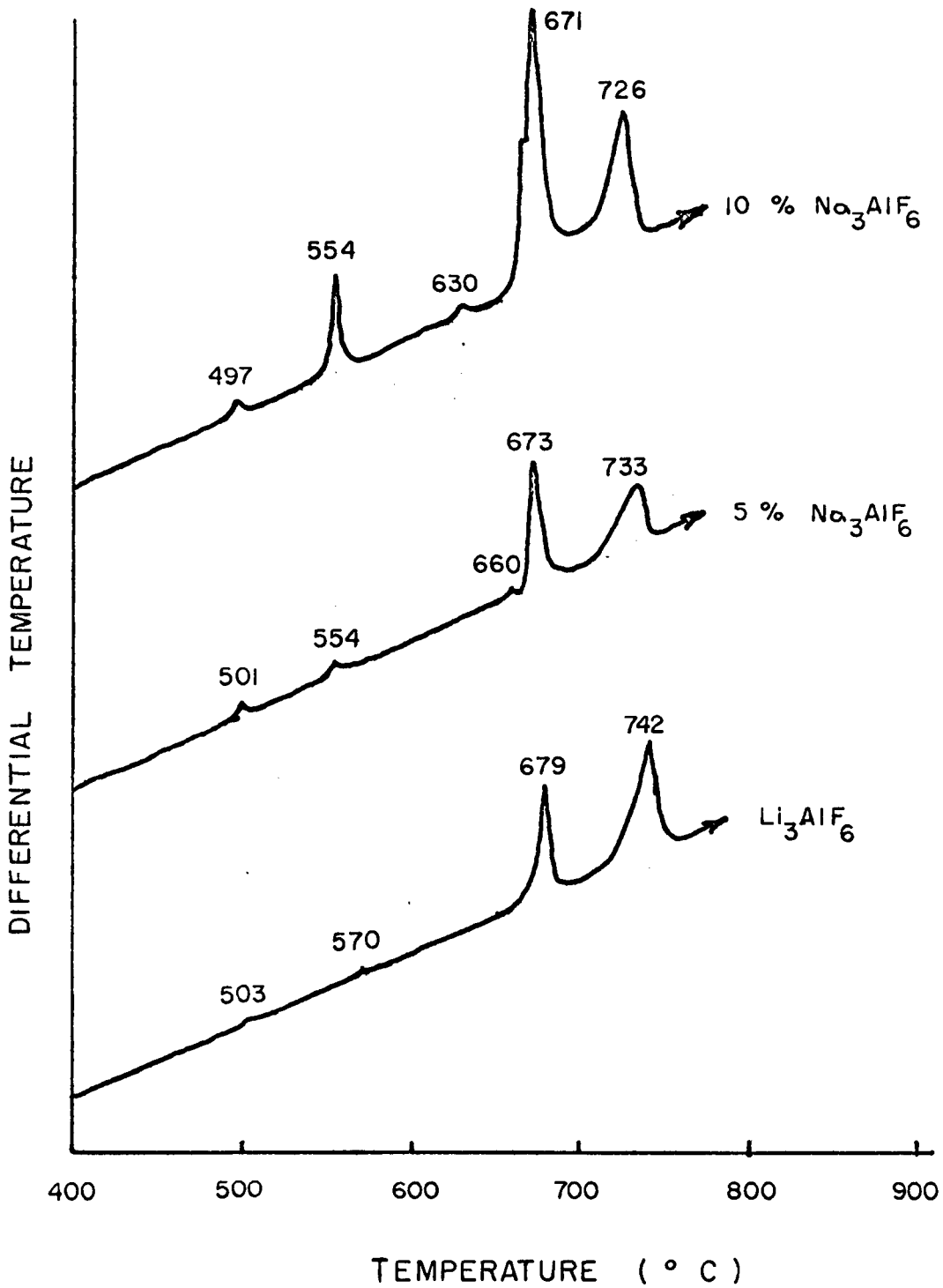

FIGURE 14. COMPARISON OF DTA PEAKS OF Li_3AlF_6 RICH COMPOSITIONS

The peak of the eutectic is small for higher Li_3AlF_6 compositions and increases to a very large peak near the eutectic as expected. The eutectic temperature shown by these DTA peaks is 670°C.

Other features to note in this diagram include a eutectoid at 505°C, a peritectic at 730°C, and a eutectic reaction at 33% Na_3AlF_6 and 685°C. The eutectoid exists at 38% Na_3AlF_6 where Na_2LiAlF_6 and $Na_3Li_3Al_2F_{12}$ are in equilibrium with $\alpha'Na_3AlF_{6(ss)}$. A peritectic reaction isotherm exists where α'-$Na_3AlF_{6(ss)}$ converts on heating to α-$Na_3AlF_{6(ss)}$ + liquid. The eutectic reaction occurs at a temperature slightly lower than most reports show but this difference is not great. The liquidus temperature recorded represents the average temperature of the liquidus peaks on one heating and one cooling curve. If only the heating curve was used the temperature is close to that reported by others. The low temperatures recorded on cooling indicate that some supercooling of the melt has taken place. The 30% Na_3AlF_6 run on the DTA is shown in Figure 15. The liquidus peak on cooling is very abrupt and at a much lower temperature than adjacent compositions confirming the possibility of supercooling.

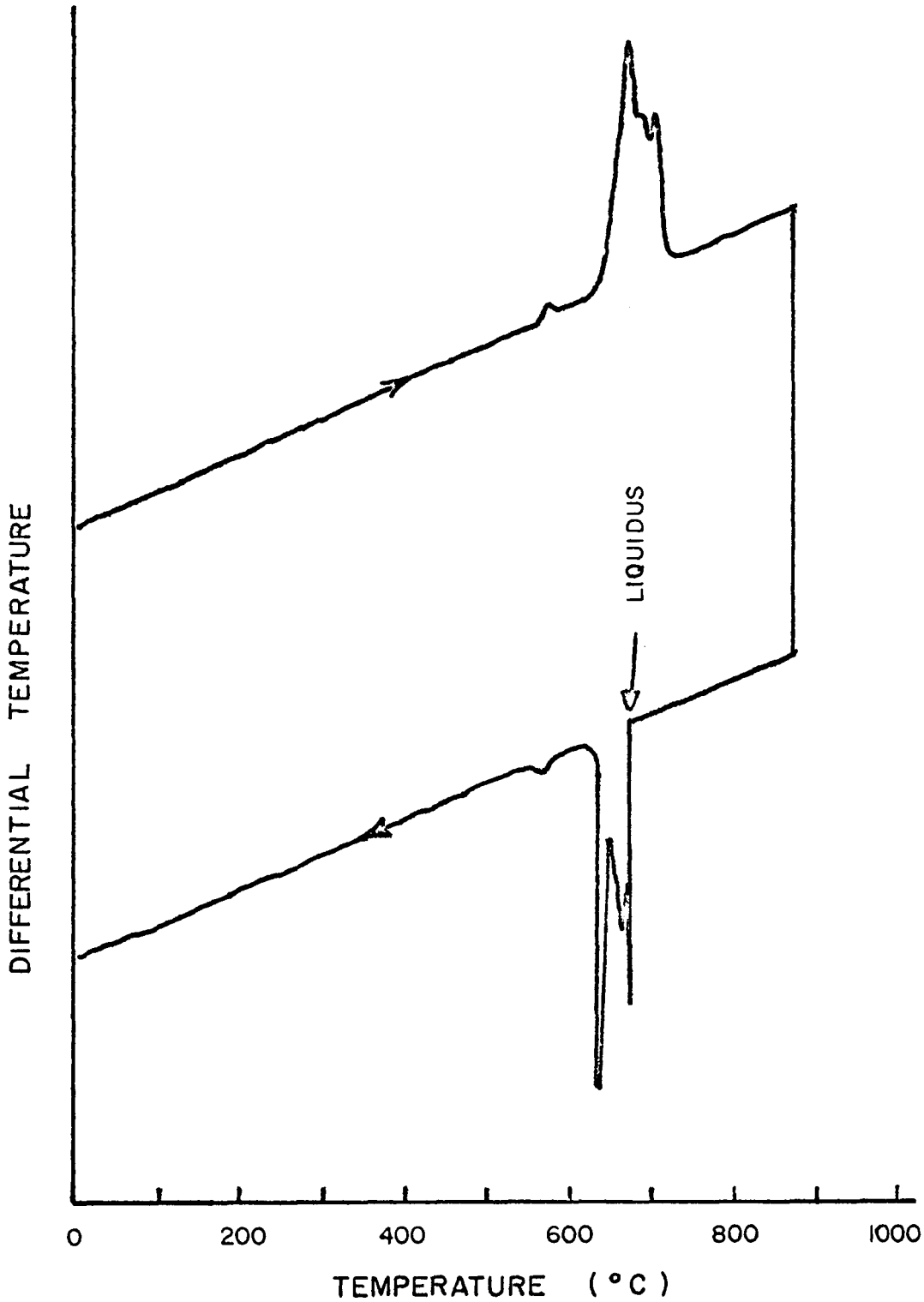

FIGURE 15. DTA PATTERN FOR A 30% Na_3AlF_6 COMPOSITION

V. SUMMARY

The phase equilibria relations in the system Na_3AlF_6-AlF_3-LiF have been examined at 500°C and on the liquidus surface. Several features of special interest include:

1) Two ternary compounds, Na_2LiAlF_6 and $Na_3Li_3Al_2F_{12}$, which decompose at 510 ± 5°C and 660 ± 5°C, respectively.

2) Seven primary phase fields which exist on the liquidus surface.

3) Three ternary eutectics which occur at 81% LiF, 9.5% Na_3AlF_6, and 9.5% AlF_3, and 685°C; 56% LiF, 6% Na_3AlF_6, and 38% AlF_3 and 585°C; 37% LiF, 17% Na_3AlF_6 and 46% AlF_3 and 620°C.

4) Extensive solid solution of Li_3AlF_6 in β-Na_3AlF_6 which exists up to 18 mole % Li_3AlF_6.

5) An intermediate solid solution which exists in the Na_3AlF_6-Li_3AlF_6 binary diagram.

BIBLIOGRAPHY

1. Mantell, C. L., Electrochemical Engineering, McGraw-Hill Book Company, Inc., New York (1960).

2. Frank, W. B. and Foster, L. M., "Constitution of Cryolite in Sodium Fluoride-Aluminum Fluoride Melts," J. Phys. Chem., 64, 95-98 (1960).

3. Grjothiem, K., "Theory of Aluminum Electrolysis," Kgl. Nor. Nor. Vidensk. Selskabs Skrifter, 2, (5), 1-90 (1957).

4. Brynestad, J., Grjotheim, K., and Urnes, S., Z. Elektrochem., 63, 707 (1959).

5. Foster, P. A., Jr. and Frank, W. Z., "The Structure of Cryolite-Alumina Melts," J. Electrochem. Soc., 107 (12), 997-1001 (1960).

6. Treadwell, W. D., Schwiez, Arch. Angew. Wiss. u. Tech., 6, Series 12, 970 (1951).

7. Rolin, M., Ann. phys., 6, Series 12, 970 (1951).

8. Frejacques, M., Ball, soc. franc. electriciens, 9, 684 (1949).

9. Dewing, E. W., Discussion of "The Structure of Cryolite-Alumina Melts" by Foster, P. A., Jr. and Frank, W. B. (J. Electrochem. Soc., 107 (12), 997-1001 (1960)), J. Electrochem. Soc., 108 (6), 611-612 (1961).

10. Forland, T., Storegroven, H., and Urnes, S., Z. anorg. V. allgem. Chem., 279, 205 (1955).

11. Boner, J. F., Helv. Chem. Acta, 33, 1137 (1950).

12. "A Revolutionary Alcoa Process," Business Week, 92-93 (January 30, 1973).

13. Frank, W. B. "Thermodynamic Considerations in the Aluminum-Producing Electrolyte," J. Phys. Chem., 65 (11), 2081-2087 (1961).

14. Pauly, Hans, "Ralstonite from Ivigtut, South Greenland," Am. Mineralogist, 50 (11-12), 851-864 (1965).

15. Garton, G. and Wanklyn, B. M., "Reinvestigation of the system Na_3AlF_6-Li_3AlF_6," J. Am. Cer. Soc., 50 (8), 395-399 (1967).

16. Fedotiev, P. P. and Ibyinskii, V., "Electrometallurgy of Aluminum," Z. Arorg. Chem., 80, 113-154 (1913).

17. Naray-Szabo, Istvan and Sigmond, Gy., "Fusion Curve of the System Cryolite-Potassium Cryolite," Mat. Termesz. Ertes., 60, 364-372 (1941).

18. Phillips, N. W. F., Singleton, P. H., and Hollengshead, E. A., "Liquidus Curves for Aluminum Cell Electrolysis: I," J. Electrochem. Soc., 102 (11), 648-649 (1955).

19. Grjotheim, Kai, "Contribution to Theory of the Aluminum Electrolysis," Norwegian Technical Institute, Trondheim, Norway, p. 18 (1956).

20. Petit, G., "Cryoscopic Study of Solutions of Certain Metallic Oxides in the Eutectic Cryolite-Sodium Fluoride," Compt. Rend., 234, 1281-1283 (1952).

21. Holm, J. L., "Structural Interpretation of the System Cryolite + Sodium aluminate," Trans. Faraday Soc., 58 (474), 1104-1107 (1962).

22. Landon, G. J. and Ubbelohde, A. R., "Melting and Crystal Structure of Cryolite ($3NaF \cdot AlF_3$)," Proc. Roy. Soc. (London), A240 (1221), 160-172 (1957).

23. Rolin, M., "Ionic Structure of Fused Pure Cryolite: II," Bull. Soc. Chim. France, 671-677 (1960).

24. Foster, P. A., Jr., "A Cryolite Melting Point Through Quenching Methods," J. Phys. Chem., 61 (7), 1005-1006 (1957).

25. Foster, P. A., Jr., "Melting Point of Cryolite," J. Am. Cer. Soc., 51 (2) 107-109 (1968).

26. Grjotheim, K., Halvorsen, T. and Urnes, S., Z. Elektrochem., 63, 707 (1959).

27. O'Brien, C. J. and Kelley, K. K., J. Am. Chem. Soc., 79, 5615 (1957).

28. Albright, D. M., Thesis, Carnegie Institute of Technology (1956).

29. Fenerty, A. and E. A. Hollingshead, "Liquidus Curves for Alumina Cell Electrolyte: III," J. Electrochem. Soc., 107 (12), 993-997 (1960).

30. Holm, J. L., "Investigation of Structure and Phase Ratio of Some Systems in Connection with Alumina Electrolysis," Norwegian Technical Institute, Trondheim, Norway, pp. 7-13 (1963).

31. Ginsberg, H. and Wefers, K., "Thermochemical Investigations in the System $NaF-AlF_3$," Erzmetall, 20 (4), 156-161 (1967).

32. Foster, P. A., Jr., "Phase Equilibria in the System $Na_3AlF_6-AlF_3$," J. Am. Cer. Soc., 53 (11), 598-600 (1970).

33. Holm, J. L. and Holm B. J., "Phase Relations and Thermodynamic Properties in the Ternary Reciprocal System $LiF-NaF-Na_3AlF_6-Li_3AlF_6$," Thermochimica Acta, 6, 375-398 (1973).

34. Holm, J. L. and Jenssen, "A Note on the Polymorphy and Structure of Li_3AlF_6," Acta Chemica Scandinavica, 23, 1065-1068 (1969).

35. Fedotieff, V. P. P. and K. Timofeeff, "Schmelzitiagramme der Systeme $KF-AlF_3$ und $LiF-AlF_3$," Z. Anorg. u. Allgem Chem., 206, 263-266 (1932).

36. Belyayer, A. I., "Electrolyte of Aluminum Cells," Metallurgizet, Moscow (1961).

37. Lewis, R. A., Process Metallurgy Division Monthly Report, (May, 1948).

38. Foster, P. A., Jr., "The Phase Diagram of the Na_3AlF_6-LiF System," Unpublished Data, Aluminum Company of America, Alcoa Center, Pa. (1968).

39. Drossbach, P., "Electrometallurgy of Aluminum," Z. Elektrochem., 42 (1), 65-70 (1936).

40. Mashovets, V. P. and Petrov, V. I., "Phase Diagram of the System $Na_3AlF_6-Li_3AlF_6-Al_2O_3$," Zh. Prikl. Khim., 30 (11), 1695-1698 (1957).

41. Rolin, M. and Muhlethaler, R., "Study of the System $Na_3AlF_6-Li_3AlF_6$ and the Dissolution of Al_2O_3 in it," Bull. Soc. Chim. France, 10, 2593-2599 (1964).

42. Holm, J. L. and Holm, B. J., "Phase Investigations in the System $Na_3AlF_6-Li_3AlF_6$," Acta Chemica Scandinavia, 24, 2535-2545 (1970).

APPENDIX A

Computer program for least squares regression analysis

```
/*MAIN  TIME=5,CARDS=1,LINES=1,REGION=150
/*PRIORITY STANDARD
//  EXEC  SAS
//SYSIN  DD  *
DATA RAB123
INPUT X1 2-6 Y1 10-15;
X1X1=X1*X1;
CARDS;
21 OBSERVATIONS IN DATA SET RAB123 3 VARIABLES
PROC REGR;
MODEL Y1=X1;
MODEL Y1=X1 X1X1;
/*
//
```

STATISTICAL ANALYSIS SYSTEM

Analysis of Variance Table, Regression Coefficients,
and Statistics of Fit for Dependent Variable Y1

Source	DF	Sum of Squares	Mean Square	F Value	Prob F	R-Square	C.V.
Regression	1	0.00036994	0.00036994	3807.63255	0.0001	0.99503480	0.01609 %
Error	19	0.00000185	0.00000010				
Corrected Total	20	0.00037179				Std Dev	Y1 Mean
						0.00031170	1.93679

Source	DF	Sequential SS	F Value	Prob F	Partial SS	F Value	Prob F
X1	1	0.00036994	3807.63255	0.0001	0.00036994	3807.63255	0.0001

Source	B Values	T for H0:B=0	Prob T	Std Err B	Std B Values
Intercept	1.94203233	15493.19363	0.0001	0.00012535	0.0
X1	-0.00068648	-18.04406	0.0001	0.00003804	-0.97639586
X1X1	-0.00000096	-0.40987	0.6867	0.00000233	-0.02217884

Source	DF	Sum of Squares	Mean Square	F Value	Prob F	R-Square	C.V.
Regression	1	0.00036994	0.00036994	3807.63255	0.0001	0.99503480	0.01609 %
Error	19	0.00000185	0.00000010				
Corrected Total	20	0.00037179				Std Dev	Y1 Mean
						0.00031170	1.93679

Source	DF	Sequential SS	F Value	Prob F	Partial SS	F Value	Prob F
X1	1	0.00036994	3807.63255	0.0001	0.00036994	3807.63255	0.0001

Source	B Values	T for H0:B=0	Prob T	Std Err B	Std B Values
Intercept	1.94205568	17787.50909	0.0001	0.00010918	0.0
X1	-0.00070133	-61.70602	0.0001	0.00001137	-0.99751431

The vita has been removed from the scanned document

PHASE EQUILIBRIA IN THE $LiF-AlF_3-Na_3AlF_6$ SYSTEM

by

David P. Stinton

(ABSTRACT)

The phase equilibria relationships in the $Na_3AlF_6-AlF_3-LiF$ ternary system have been investigated using a combination of quenching, optical microscopy, DTA, and x-ray powder diffraction techniques. The compatability relations at 500°C, the binary system $Na_3AlF_6-Li_3AlF_6$, and the ternary liquidus surface were determined. The liquidus surface was found to contain the following five important invariant points:

1) eutectic - 81% LiF, 9.5% Na_3AlF_6, 9.5% AlF_3 and 685°C
2) eutectic - 56% LiF, 6% Na_3AlF_6, 38% AlF_3 and 585°C
3) eutectic - 37% LiF, 17% Na_3AlF_6, 46% AlF_3 and 620°C
4) peritectic - 30% LiF, 37% Na_3AlF_6, 33% AlF_3 and 660°C
5) reaction point - 65% LiF, 9% Na_3AlF_6, 26% AlF_3 and 675°C

The 500°C isothermal section contains 7 three-phase regions and 2 large two-phase regions. The binary system $Na_3AlF_6-Li_3AlF_6$ contained 2 incongruently melting compounds, many polymorphic transformations, and a eutectic at 690°C and 67 mole % Li_3AlF_6.